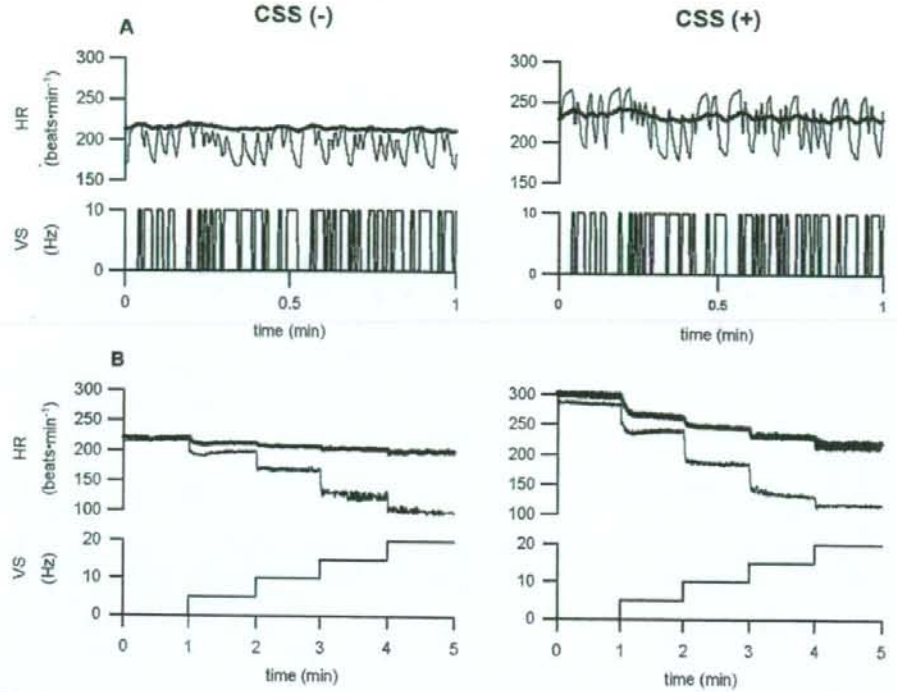

Fig. 1. A: Representative recordings of HR obtained utilizing binary white-noise vagal stimulation (top) and the corresponding vagal stimulation (VS; bottom) without (left) and with (right) CSS. Thin line, control; thick line, K_{ACh} channel blockade with tertiapin (30 nmol·kg^{-1} iv). **B**: Representative recordings of HR obtained utilizing stepwise vagal stimulation (top) and the corresponding VS (bottom) without (left) and with (right) CSS, which increased the basal HR and the amplitude of HR variation in both binary white-noise and stepwise vagal stimulations. A K_{ACh} channel blockade attenuated the amplitude of HR variation and the speed of the response of HR to vagal stimulation regardless of CSS.

Table 1. Effects of tertiapin infusion and CSS on AP and HR before and during dynamic vagal stimulation.

	CSS (–)		CSS (+)		Comparison factors		
	Control	Tertiapin	Control	Tertiapin	Drug	CSS	Interaction
AP, mmHg							
Before stimulation	82.2 ± 16.8	76.7 ± 20.1	90.5 ± 13.8	81.8 ± 16.6	0.022	0.641	0.546
During stimulation	80.2 ± 18.4	76.6 ± 21.4	81.8 ± 14.8	75.9 ± 19.0	0.144	0.962	0.709
HR, beats·min^{-1}							
Before stimulation	247.8 ± 20.1	247.9 ± 30.8	312.2 ± 15.6	307.4 ± 20.9	0.521	<0.001	0.494
During stimulation	211.9 ± 17.5**	228.3 ± 23.4	244.3 ± 33.3**	248.1 ± 30.7**	0.026	<0.001	0.308

Values are means ± SD (n = 7). CSS, cardiac sympathetic stimulation; AP, arterial pressure; HR, heart rate. **P < 0.01 vs. corresponding values before stimulation. Tertiapin was infused at 30 nmol/kg iv.

input signal and not the vagal stimulation frequency itself. Table 2 summarizes parameters of the transfer function at 0.01, 0.1, 0.5, and 1 Hz and also those of the step response. Tertiapin attenuated the dynamic gain compared with the control conditions regardless of CSS. The phase approached –Π radians at the lowest frequency and lagged with increasing frequency under the control conditions. Tertiapin increased the phase delay in the frequency range from 0.01 to 1 Hz. Coherence was near unity in the overall frequency range under the control conditions. A decrease in the coherence function from unity was noted >0.6 Hz under the condition of the K_{ACh} channel blockade, which was reversed by CSS.

Figure 2B shows the calculated step response of HR to vagal stimulation averaged for all animals under the conditions of control (thin lines) and K_{ACh} channel blockade

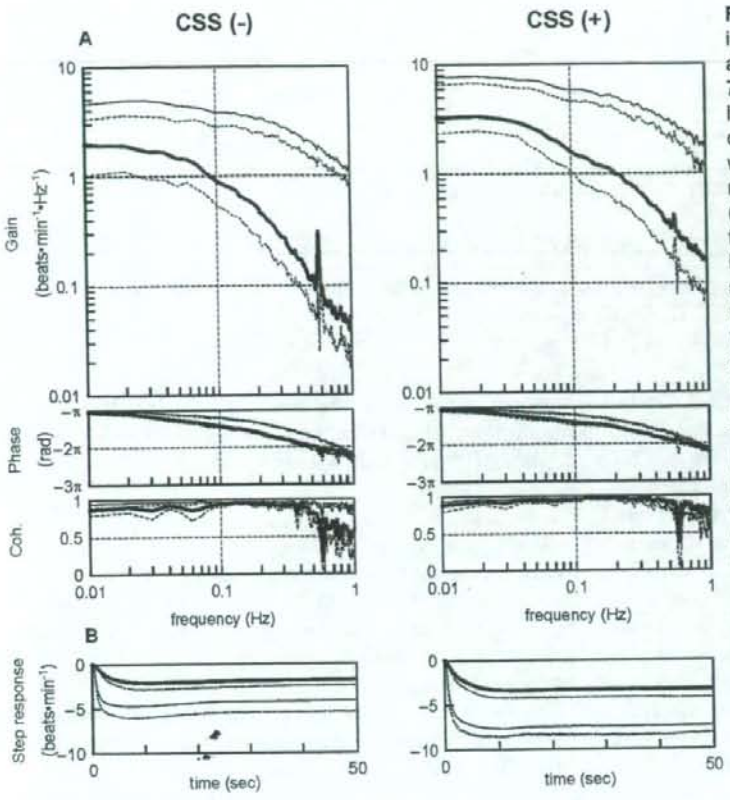

Fig. 2. A: Dynamic transfer function relating vagal stimulation to the HR responses averaged from all animals (pooled data; n = 7) without (left) and with (right) CSS. Solid lines, means; dashed lines, –SD. Thin line, control; thick line, a K_{ACh} channel blockade with tertiapin (30 nmol·kg^{-1} iv). Top: gains; middle: phase shifts; bottom: coherence (Coh) functions. Tertiapin decreased transfer gain and increased the phase shift with increasing frequency. Cardiac sympathetic stimulation increased transfer gain both under control conditions and under conditions of a K_{ACh} channel blockade without affecting the phase shift. **B**: Calculated step response to 1 Hz tonic vagal stimulation averaged from all animals (pooled data; n = 7) without (left) and with (right) CSS. Solid lines, means; dashed lines, –SD. Thin line, control; thick line, K_{ACh} channel blockade with tertiapin (30 nmol·kg^{-1} iv). The K_{ACh} channel blockade decreased the maximum step response and slowed the initial step response. CSS increased the maximum step response both under control conditions and under conditions of a K_{ACh} channel blockade without affecting the initial response (see Table 2).

Table 2. Effects of tertiapin infusion and CSS on parameters of the transfer function and step response.

	CSS (–)		CSS (+)		Comparison factors		
	Control	Tertiapin	Control	Tertiapin	Drug	CSS	Interaction
Gain, beats·min^{-1}·Hz^{-1}							
0.01 Hz	4.58 ± 1.26	2.21 ± 0.97	7.73 ± 1.15	3.28 ± 0.92	<0.001	0.001	0.007
0.1 Hz	3.81 ± 1.01	1.10 ± 0.43	5.82 ± 1.28	1.60 ± 0.54	<0.001	0.007	0.015
0.5 Hz	2.12 ± 0.64	0.16 ± 0.07	3.08 ± 0.82	0.36 ± 0.17	<0.001	0.013	0.081
1 Hz	1.09 ± 0.27	0.08 ± 0.03	1.73 ± 0.61	0.16 ± 0.08	<0.001	0.019	0.044
Phase, rad							
0.01 Hz	3.10 ± 0.04	2.99 ± 0.11	2.99 ± 0.11	2.92 ± 0.14	0.037	0.077	0.579
0.1 Hz	2.52 ± 0.08	1.78 ± 0.17	2.52 ± 0.11	1.83 ± 0.25	<0.001	0.757	0.719
0.5 Hz	0.91 ± 0.13	0.03 ± 0.27	0.90 ± 0.10	0.35 ± 0.10	<0.001	0.011	0.056
1 Hz	–0.56 ± 0.33	–0.81 ± 0.21	–0.41 ± 0.26	–0.64 ± 0.18	0.014	0.159	0.905
Coherence							
0.01 Hz	0.95 ± 0.05	0.87 ± 0.07	0.93 ± 0.04	0.89 ± 0.09	0.005	0.947	0.424
0.1 Hz	0.96 ± 0.03	0.94 ± 0.04	0.97 ± 0.01	0.95 ± 0.02	0.004	0.440	0.835
0.5 Hz	0.96 ± 0.02	0.83 ± 0.08	0.91 ± 0.08	0.93 ± 0.04	0.026	0.259	0.006
1 Hz	0.90 ± 0.07	0.59 ± 0.16	0.78 ± 0.15	0.79 ± 0.12	0.017	0.312	0.011
Maximum step response, beats·min^{-1}	–4.2 ± 1.2	–1.8 ± 0.6	–7.4 ± 0.9	–3.3 ± 0.9	<0.001	<0.001	0.005
Time constant, s	0.63 ± 0.09	3.34 ± 0.55	0.74 ± 0.18	3.18 ± 1.10	<0.001	0.913	0.560

Values are means ± SD (n = 7). CSS, cardiac sympathetic stimulation. Tertiapin was infused at 30 nmol/kg iv.

Table 3. Effects of tertiapin infusion and CSS on parameters of the transfer function relating dynamic vagal stimulation to HR.

	CSS (–)		CSS (+)		Comparison factors		
	Control	Tertiapin	Control	Tertiapin	Drug	CSS	Interaction
Dynamic gain, beats·min^{-1}·Hz^{-1}	4.6 ± 1.1	2.3 ± 0.9	7.3 ± 1.1	3.6 ± 1.0	<0.001	<0.001	0.037
Corner frequency, Hz	0.26 ± 0.04	0.05 ± 0.01	0.23 ± 0.06	0.06 ± 0.02	<0.001	0.439	0.1613
Lag time, s	0.38 ± 0.04	0.45 ± 0.04	0.34 ± 0.04	0.38 ± 0.03	<0.001	0.002	0.2776

Values are means ± SD (n = 7). CSS, cardiac sympathetic stimulation; HR, heart rate. Tertiapin was infused at 30 nmol/kg iv.

(thick lines), without (left) and with (right) CSS. Tertiapin slowed the transient response and attenuated the HR response to vagal stimulation in the time domain. CSS did not affect the time constant, though it augmented the maximum step response. A significant interaction was observed between the tertiapin and CSS effects in the maximum step response, but not in the time constant (Table 2).

The fitted parameters of the transfer functions are summarized in Table 3. Tertiapin significantly decreased the dynamic gain and the corner frequency and significantly increased the lag time. Conversely, CSS significantly increased the dynamic gain and significantly decreased the lag time. A significant interaction was observed between the tertiapin and CSS effects only in dynamic gain.

Static protocol

Figure 3A summarizes changes in HR in response to stepwise vagal stimulation without (left) and with (right) CSS, which increased basal HR obtained at 0 Hz vagal stimulation by approximately 50 beats·min^{-1}. Tertiapin significantly attenuated the bradycardic response to vagal stimulation regardless of CSS. The magnitude of attenuation (i.e., the difference between the open and closed symbols) became greater as the vagal stimulation frequency increased.

Figure 3B demonstrates the HR reduction obtained under four conditions at each frequency. To aid an intuitive understanding, the tertiapin condition is designated as D(–) in this panel because tertiapin blocked the direct action of ACh. S(+) indicates the presence of CSS. At 5 Hz vagal stimulation frequency, the direct action alone S(–)D(+) significantly augmented the HR reduction, as depicted by the diagonal hatch. CSS alone S(+)D(–) also significantly augmented the HR reduction, as depicted by the vertical hatch. The augmentation of the HR reduction obtained by S(+)D(+) exceeded the simple summation of the diagonal hatch and vertical hatch, suggesting that the effect of the direct action was enhanced by CSS (depicted in the solid rectangle). The positive interaction waned at 10 Hz vagal stimulation and disappeared at 15 and 20 Hz vagal stimulation. That is, the simple summation of the diagonal hatch and vertical hatch largely explained the augmentation of the HR reduction attained by S(+)D(+) at 15 and 20 Hz vagal stimulation.

DISCUSSION

We have examined the effect of background sympathetic tone on the direct action of ACh through K_{ACh} channels by examining the dynamic and static transfer characteristics. The major findings in the present study are that the bradycardic response to vagal stimulation via the K_{ACh} channels was augmented by concomitant CSS, depending on vagal stimulation frequency. The rapidity of vagal HR control obtained by the K_{ACh} channels, however, was not affected by CSS. These findings support our hypotheses and demonstrated, for the first time to our knowledge, the existence of an accentuated antagonism in the direct action of ACh through the K_{ACh} channels.

Effect of CSS on the rapidity of vagal HR control via K_{ACh} channels

Our results indicate that the rapidity of the vagal HR control via the K_{ACh} channels was not affected by background sympathetic tone. In the transfer function, the phase values were significantly more delayed by the K_{ACh} channel blockade in the frequency range from 0.01 to 1 Hz in agreement with our previous study [6]. In contrast, CSS did not affect the phase characteristics, in which no significant interaction was observed at each frequency (Table 2). Moreover, the calculated step response clearly demonstrated that tertiapin significantly prolonged the time constant by >2 s, whereas CSS did not affect it (Fig. 2B and Table 2).

Changes in fitted parameters of the transfer function from vagal stimulation to HR also support our first hypothesis that CSS does not affect the rapidity of the vagal HR control mediated by the K_{ACh} channels. Tertiapin decreased the corner frequency to a similar degree without or with CSS, which did not affect the corner frequency. On the other hand, tertiapin prolonged the lag time, whereas CSS shortened it (Table 3). However, changes in the lag time caused by tertiapin or CSS were less than 0.1 s and might

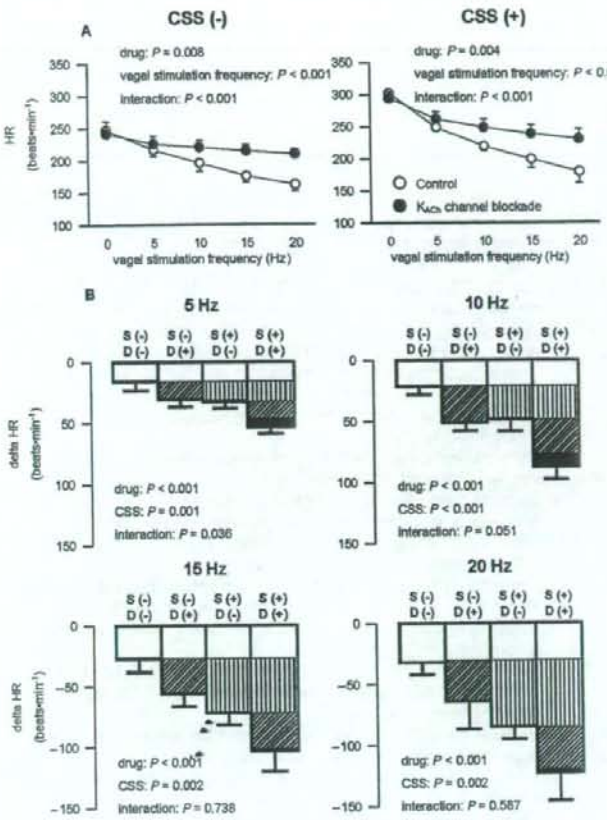

Fig. 3. A: Static HR responses relating stepwise vagal stimulation averaged from all animals (pooled data; n = 5) without (left) and with (right) CSS. A K_{ACh} channel blockade decreases the static HR response, and the static reductions in the bradycardic effect were greater at higher stimulation frequencies in both conditions. **B**: Changes in HR responses from baseline to vagal stimulation at 5 Hz (top left), 10 Hz (top right), 15 Hz (bottom left), and 20 Hz (bottom right) averaged from all animals (pooled data; n = 5). To aid an intuitive understanding, the tertiapin condition was designated as D(–) in this panel because tertiapin blocked the direct action of ACh. S(+) indicates the presence of CSS. Significant interaction and a tendency towards significant interaction (P = 0.051) were obtained at 5 and 10 Hz vagal stimulation, respectively, but not at 15 and 20 Hz vagal stimulation.

be insignificant in terms of physiological HR control.

Effect of CSS on the gain of vagal HR control via K_{ACh} channels

Because the direct action of ACh via K_{ACh} is considered to be independent of sympathetic control [12], an accentuated antagonism is unlikely to occur in the direct action. However, because the interbeat interval is determined by the pacemaker potential of the sinus node cells, which in turn depends on all of the potassium, sodium, and calcium currents, there could be interaction between the K_{ACh} channel pathway and background sympathetic tone when we observe the HR response. Changes in the sodium current and/or calcium current induced by background sympathetic tone would modify the effect of changes in the potassium current through the K_{ACh} channels.

Our results indicate that accentuated antagonism occurred, affecting the direct action of ACh in the range of mild vagal stimulation as follows. In the dynamic protocol that was carried out with a mean vagal stimulation frequency of 5 Hz, significant positive interaction was observed between the tertiapin and CSS effects, affecting the dynamic gain as well as the calculated maximum step response (Table 2), suggesting that the effect of the K_{ACh} channel pathway was enhanced during CSS. The static protocol also showed significant positive interaction at 5 Hz vagal stimulation (Fig. 3B). The augmentation of the bradycardic response to vagal stimulation gained by the direct action of ACh through the K_{ACh} channels was enhanced under concomitant CSS.

The reason for the absence of a positive interaction between the tertiapin and CSS effects at 15 and 20 Hz vagal stimulation is unclear (Fig. 3B). One possible explanation is the curvilinearity of the HR response to vagal stimulation. In the right panel of Fig. 3A, the tertiapin-free control data (open symbols), which correspond to S(+)D(+) in Fig. 3B, showed the steepest slope at the 0–5 Hz vagal stimulation step. The slope became shallower as the vagal stimulation frequency increased, suggesting a saturation phenomenon of HR reduction in response to vagal stimulation. It is very likely that such curvilinearity masked possible positive interaction between CSS and the direct action of ACh in determining the HR reduction during 15 and 20 Hz vagal stimulation. Accentuated antagonism in the direct action of ACh through K_{ACh} channels might therefore operate under balanced conditions of sympa-

thetic and vagal nerve activities.

The existence of an accentuated antagonism in the direct action of ACh through the K_{ACh} channels could be explained by macromolecular signaling complexes in which G protein-gated inwardly rectifying potassium (GIRK) channels are physically associated with signaling partner regulated by different G protein-coupled receptors (GPCRs) [19, 20]. Cardiac sympathetic stimulation simultaneously activates several different GPCRs: α-adrenergic, β1-adrenergic, and β2-adrenergic receptors. Notably, the β1-adrenergic receptor is coupled to downstream kinase, protein kinase A (PKA). The β-adrenergic signaling via PKA phosphorylation increases the activity of K_{ACh} channels [21, 22]. Taken together, β-adrenergic receptors might augment the activity of K_{ACh} channels via a PKA-dependent mechanism.

Limitations

This study has several limitations. First, the data was obtained from anesthetized animals. Since anesthesia would affect the autonomic tone, the results may not be directly applicable to conscious animals. However, because we cut and stimulated the right cardiac sympathetic and vagal nerves, changes in autonomic outflow associated with anesthesia might not have significantly affected the present results.

Second, we blocked the K_{ACh} channels to examine the effect of background sympathetic tone on the direct effect of ACh through the K_{ACh} channels. On the other hand, if we had blocked the indirect effect of ACh through the cyclic AMP pathway, leaving the direct effect of ACh intact, and then examined the effect of background sympathetic tone on the HR response to vagal stimulation, the results might have been excessively straightforward. However, we could find no blocker for the indirect effect of ACh alone that was suitable for in vivo study at present. Further studies are required to directly examine the effect of background sympathetic tone on the direct effect of ACh through the K_{ACh} channels.

In conclusion, concomitant CSS affected no parameters of rapidity (i.e., the corner frequency in the frequency domain and the time constant in the time domain) of vagal HR control via K_{ACh} channels. Moreover, HR reduction in response to vagal stimulation via K_{ACh} channels was augmented by concomitant sympathetic stimulation at 5 Hz vagal stimulation. These findings suggest that the rapidity of response of the vagal HR control via K_{ACh} channels is invariant with respect to background sympathetic tone, and that the magnitude of vagal HR control via K_{ACh} channels is affected by background sympathetic tone in vivo.

This study was supported by Health and Labour Sciences Research Grants H15-Physi-001, H18-Nano-Ippan-003, and H18-Iryo-Ippan-023 from the Ministry of Health, Grants-in-Aid for Scientific Research promoted by the Ministry of Education, Culture, Sports, Science and Technology in Japan 18591992, 19700559, and by the Ground-based Research Announcement for Space Utilization project promoted by the Japan Space Forum. This study was also supported by an Industrial Technology Research Grant Program in 06B44524a from the New Energy and Industrial Technology Development Organization of Japan.

REFERENCES

1. Luetje CW, Tietje KM, Christian JL, Nathanson NM. Differential tissue expression and developmental regulation of guanine nucleotide binding regulatory proteins and their messenger RNAs in rat heart. J Biol Chem. 1988;263:13357-65.
2. Sunahara RK, Dessauer CW, Gilman AG. Complexity and diversity of mammalian adenylyl cyclases. Annu Rev Pharmacol Toxicol. 1996;36:461-80.
3. Huang CL, Slesinger PA, Casey PJ, Jan YN, Jan LY. Evidence that direct binding of G beta gamma to the GIRK1 G protein-gated inwardly rectifying K+ channel is important for channel activation. Neuron. 1995;15:1133-43.
4. Sakmann B, Noma A, Trautwein W. Acetylcholine activation of single muscarinic K+ channels in isolated pacemaker cells of the mammalian heart. Nature. 1983;303:250-3.
5. Yamada M, Inanobe A, Kurachi Y. G protein regulation of potassium ion channels. Pharmacol Rev. 1998;50:723-60.
6. Mizuno M, Kamiya A, Kawada T, Miyamoto T, Shimizu S, Sugimachi M. Muscarinic potassium channels augment dynamic and static heart rate responses to vagal stimulation. Am J Physiol Heart Circ Physiol. 2007;293:H1564-70.
7. Negrão CE, Rondon MU, Tinucci T, Alves MJ, Roveda F, Braga AM, Reis SF, Nastari L, Barretto AC, Krieger EM, Middlekauff HR. Abnormal neurovascular control during exercise is linked to heart failure severity. Am J Physiol Heart Circ Physiol. 2001;280:H1286-92.
8. Mancia G, Grassi G, Giannattasio C, Seravalle G. Sympathetic activation in the pathogenesis of hypertension and progression of organ damage. Hypertension. 1999;34:724-8.
9. Seals DR, Bell C. Chronic sympathetic activation: consequence and cause of age-associated obesity? Diabetes. 2004;53:276-84.
10. Hartzell HC, Méry PF, Fischmeister R, Szabo G. Sympathetic regulation of cardiac calcium current is due exclusively to cAMP-dependent phosphorylation. Nature. 1991;351:573-6.
11. Irisawa H, Brown HF, Giles W. Cardiac pacemaking in the sinoatrial node. Physiol Rev. 1993;73:197-227.
12. Breitwieser GE, Szabo G. Uncoupling of cardiac muscarinic and beta-adrenergic receptors from ion channels by a guanine nucleotide analogue. Nature. 1985;317:538-40.
13. Levy MN. Sympathetic-parasympathetic interactions in the heart. Circ Res. 1971;29:437-45.
14. Kawada T, Ikeda Y, Sugimachi M, Shishido T, Kawaguchi O, Yamazaki T, Alexander J Jr, Sunagawa K. Bidirectional augmentation of heart rate regulation by autonomic nervous system in rabbits. Am J Physiol. 1996;271:H288-95.
15. Kawada T, Uemura K, Kashihara K, Jin Y, Li M, Zheng C, Sugimachi M, Sunagawa K. Uniformity in dynamic baroreflex regulation of left and right cardiac sympathetic nerve activities. Am J Physiol Regul Integr Comp Physiol. 2003;284:R1506-12.
16. Brigham E. FFT transform applications. In: The Fast Fourier Transform and its applications. Englewood Cliffs, NJ: Prentice Hall; 1988. p. 167-203.
17. Bendat J, Piersol A. Single-input/output relationships. In: Random data: analysis and measurement procedures (3rd edition). New York: Wiley; 2000. p. 189-217.
18. Marmarelis P, Marmarelis V. The white noise method in system identification. In: Analysis of physiological systems. New York: Plenum; 1978. p. 131-221.
19. Lavine N, Ethier N, Oak JN, Pei L, Liu F, Trieu P, Rebois RV, Bouvier M, Hebert TE, Van Tol HH. G protein-coupled receptors form stable complexes with inwardly rectifying potassium channels and adenylyl cyclase. J Biol Chem. 2002;277:46010-9.
20. Nikolov EN, Ivanova-Nikolova TT. Coordination of membrane excitability through a GIRK1 signaling complex in the atria. J Biol Chem. 2004;279:23630-6.
21. Kim D. Beta-adrenergic regulation of the muscarinic-gated K+ channel via cyclic AMP-dependent protein kinase in atrial cells. Circ Res. 1990;67:1292-8.
22. Müllner C, Vorobiov D, Bera AK, Uezono Y, Yakubovich D, Frohnwieser-Steinecker B, Dascal N, Schreibmayer W. Heterologous facilitation of G protein-activated K(+) channels by beta-adrenergic stimulation via cAMP-dependent protein kinase. J Gen Physiol. 2000;115:547-58.

30th Annual International IEEE EMBS Conference
Vancouver, British Columbia, Canada, August 20-24, 2008

Modification of Autonomic Balance by Electrical Acupuncture does not Affect Baroreflex Dynamic Characteristics

Masaru Sugimachi, *Member, IEEE*, Toru Kawada,
Hiromi Yamamoto, Atsunori Kamiya,
Tadayoshi Miyamoto, and Kenji Sunagawa, *Member, IEEE*

Abstract— *Background:* **We have demonstrated that modification of autonomic balance by electrical vagal stimulation delays progression of cardiac dysfunction and cardiac remodeling, and prolongs survival in rats with severe heart failure. We have also shown that we were able to modify autonomic balance by electrical acupuncture at the acupoint of Zusanli, potentially applicable for the treatment of heart failure. We examined the effect of the acupuncture on the dynamic characteristics of the baroreflex system to exclude the possible deleterious effect on orthostatic tolerance.**

Method: **In anesthetized 8 and 6 rabbits, we examined static and dynamic characteristics of baroreflex, respectively, with and without electrical acupuncture (1 Hz, 5 mA, and 5msec). Dynamic characteristics were examined by imposing pseudorandom binary changes in isolated carotid sinus pressure.**

Results: **With the stimulation condition to decrease arterial blood pressure and sympathetic nerve activity (resulted form decreased response range of neural arc), either of the dynamic characteristics of neural arc or those of peripheral arc did not change by electrical acupuncture at Zusanli.**

Conclusion: **We conclude that application of electrical acupuncture at Zusanli can suppress sympathetic nerve activity but does not affect the dynamic characteristics of the arterial baroreflex system, indicating no deleterious effect on orthostatic tolerance.**

Manuscript received April 7, 2008. This work was supported in part by Health and Labour Sciences Research Grants (H19-nano-ippan-009, H15-physi-001) from the Ministry of Health Labour and Welfare of Japan, and by the Program for Promotion of Fundamental Studies in Health Science of the National Institute of Biomedical Innovation.

M. Sugimachi, D. Michikami, T. Kawada, H. Yamamoto, and A. Kamiya are with the National Cardiovascular Center Research Institute, Suita, Osaka 5658565, Japan (corresponding author Masaru Sugimachi to provide phone: +81-6-6833-512; fax: +81-6-6835-5403; e-mail: su91mach@ri.ncvc.go.jp).

D. Michikami is supported by a postdoctoral program by Japan Association for the Advancement of Medical Equipment.

T. Miyamoto is with Morinomiya University of Medical Sciences, Osaka 5590034 Japan. (e-mail: miyamoto@morinomiya-u.ac.jp).

K. Sunagawa is with Kyushu University Graduate School of Medical Sciences, Fukuoka 8128582 Japan. (e-mail: sunagawa@cardiol.med.kyushu-u.ac.jp).

I. INTRODUCTION

It is widely accepted that chronic heart failure involves not only abnormal structural and functional changes of heart and vessels themselves, but also abnormal changes in cardiovascular regulation. The fact that all successful cardiovascular drugs (ACE inhibitors, beta-adrenergic blockers, angiotensin receptor blockers, and aldosterone inhibitors) recently developed to treat heart failure are aimed at antagonizing neurohumoral activation has supported this.

We have shown that modification of autonomic balance by direct electrical vagal stimulation has inhibited cardiac remodeling, further deterioration of cardiac function, and improved survival in rat model of post-infarction severe chronic heart failure [1]. Because of the poor prognosis of chronic heart failure even with the use of combination of medical therapy, device-based therapy and the current state-of-art therapeutic modalities, such as cardiac transplantation, artificial heart, development of an additional therapeutic strategy attacking the abnormal cardiovascular regulation seems of great value to help still unsaved patients.

We have also shown in the last meeting that we were able to modify autonomic balance by electrical acupuncture at the acupoint of Zusanli, which is potentially applicable to treat heart failure. The less invasive nature of the acupuncture would greatly enhance its widespread use.

In this article, we have examined the effect of the acupuncture on the dynamic characteristics of the baroreflex system to ensure that there is no deleterious effect on orthostatic tolerance. The results indicated that electrical acupuncture is able to suppress sympathetic nerve activity but does not affect the dynamic characteristics of the arterial baroreflex system.

II. MODEL AND METHODS

A. Animal Experiments

We used 8 rabbits (Japanese White) to examine the effects of electrical acupuncture on open-loop static characteristics of baroreflex system. The effects of electrical acupuncture on open-loop dynamic characteristics were examined in other 6 rabbits.

978-1-4244-1815-2/08/$25.00 ©2008 IEEE.

In both protocols, rabbits were cared for in accordance with the Guiding Principles for the Care and Use of Animals in the Field of Physiological Sciences approved by the Physiological Society of Japan. These animals were anesthetized by a mixture of urethane (250 mg/ml) and α-chloralose (40 mg/ml) with an initial dose of 2 ml/kg (iv) and additional doses to maintain an appropriate level of anesthesia. Rabbits were mechanically ventilated with oxygen-enriched room air. Pancuronium bromide (0.1 mg/kg), a muscle relaxant was administered to prevent contaminating muscular activities.

A catheter-tipped micromanometer was inserted into a femoral artery to measure arterial blood pressure. After thoracotomy, we identified a left cardiac sympathetic nerve and the peripheral end was cut. Its efferent activity was recorded by a pair of stainless steel wire electrodes attached to the central end. We used silicone glue (Kwik-Sil, World Precision Instruments, Sarasota, FL) to fix the electrode, to provide insulation and to prevent the nerve from drying. We band-pass filtered the electrical signal at 150–1000 Hz and full-wave rectified, and low-pass filtered at a cutoff frequency of 30 Hz to quantify nerve activity.

To open the negative feedback loop, we isolated both carotid sinuses from the systemic circulation. We filled the isolated carotid sinuses with warmed physiological saline for longer preservation of baroreflex function. The blind-sac carotid sinuses were connected to a servo-controlled piston pump (model ET-126A, Labworks, Costa Mesa, CA) to control the pressure imposed on baroreceptors. Although being unphysiological and making baroreflex gain lower, it was necessary to cut bilateral vagal nerves and bilateral aortic depressor nerves to make baroreflex system fully open-loop condition.

Signals such as arterial blood pressure (AP), integrated sympathetic nerve activity (SNA), and carotid sinus pressure (CSP) were simultaneously digitized by a 12-bit analog-to-digital converter interfaced with a laboratory computer, and were stored on a hard disk for offline analysis. We used an arbitrary unit for nerve activity.

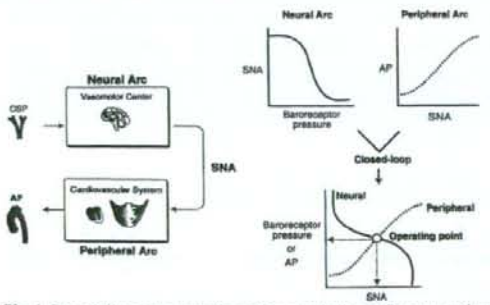

Fig. 1. Decoupling and recoupling of the arterial baroreflex system into neural arc and peripheral arc. CSP, carotid sinus pressure; AP, arterial blood pressure; SNA, sympathetic nerve activity.

B. Method to Identify Static Open-loop Characteristics of Baroreflex System

We have opened (see above) the total negative feedback loop of the arterial baroreflex system, and subdivided it into two subsystems. The two subsystems include the "neural arc" (which in turn includs baroreceptor and vasomotor center) and the "peripheral arc" (which in turn includes various sympathetic effectors). The neural arc corresponds to the controller and the peripheral arc corresponds to the plant of the baroreflex feedback system [2].

To quantify the static characteristics, we imposed stepwise change in CSP from 40 mmHg to 160mmHg with an increment of 20 mmHg. The particular CSP level was maintained for 60 seconds and the steady-state CSP, SNA, and AP were quantified by averaging the digitized values for the last 10 seconds.

We have characterized the neural arc by the relationship between CSP and SNA. We have characterized the peripheral arc by the relationship between SNA and AP. By recoupling these curves we can determine the operating point of the baroreflex system under the closed-loop condition by the intersection between the neural and peripheral arc curves.

C. Method to Identify Dynamic Open-loop Characteristics of Baroreflex System

We identified the dynamic characteristics of baroreflex, with or without electrical acupuncture. We imposed CSP changes around the respective closed-loop operating point with the amplitude of 20 mmHg according to a pseudorandom binary sequence.

The wideband nature of white noise input allows estimation of the wideband system dynamic properties. In addition, we ensemble-averaged the input power and cross power across multiple segments to reduce the statistical variance [3, 4].

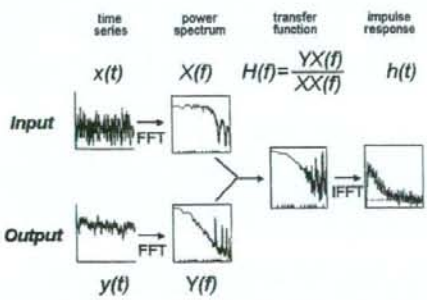

Fig. 2. Method to identify dynamic characteristics of a system. x(t), input signal; y(t), output signal; X(f) and Y(f), amplitude spectrum of x(t) and y(t), respectively; XX(f) and YX(f), ensemble-averaged input power spectrum and cross power (between input and output) spectrum, respectively; H(f), transfer function; h(t), impulse response.

We identified neural arc dynamic characteristics by analyzing CSP as input and SNA as output. We also identified peripheral arc dynamic characteristics by analyzing SNA as input and AP as output. Total baroreflex dynamic characteristics were obtained by analyzing CSP as input and AP as output.

In reference to Fig. 2, both input [x(t)] and output [y(t)] signals are divided into multiple segments. These data are subjected to frequency analysis using a fast Fourier transform (FFT) algorithm [X(f) and Y(f)]. The calculated input power and cross power (between input and output signals) are ensemble-averaged across segments to reduce variance [XX(f) and YX(f)]. Finally the transfer function [H(f)] is obtained by dividing the ensembled cross power by the ensembled input power. The impulse response [h(t)] is calculated by the inverse FFT of the transfer function.

D. Electrical Acupuncture

We have performed electrical acupuncture at Zusanli, i.e., the one-fifth point (from the knee) with the use of a pair of stainless steel wires (0.2 mm in diameter). The midpoint of the knee-ankle distance of approximately 30–35 mm served as the reference electrode. These needles were inserted to a depth of 10 mm in the skin and underlying muscle (the tibialis anterior muscle) [5].

The effects of Zusanli stimulation on baroreflex neural and peripheral arc characteristics were studied with the stimulation condition of 1 Hz, 5 mA, and 5msec. The stimulation condition is based on preliminary experiments.

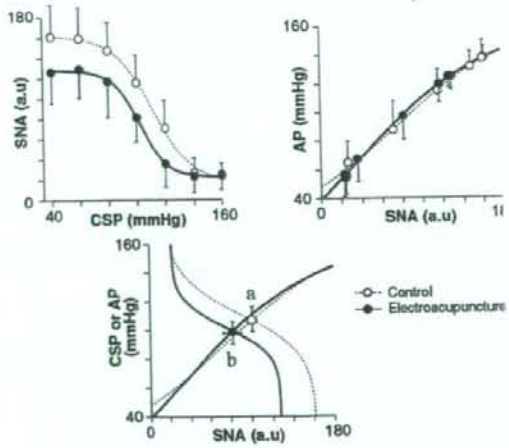

Fig. 3. Effect of electrical acupuncture on neural arc (top left) and peripheral arc (top right) static characteristics of arterial baroreflex, superimposed neural and peripheral arc curves (bottom). CSP, carotid sinus pressure; AP, arterial blood pressure; SNA, sympathetic nerve activity; solid line, with electrical acupuncture; dashed line, without electrical acupuncture, error bars, 1SD.

III. Results

A. Effects on Static Characteristic

The response range of SNA for the CSP change of 40-160 mmHg was obviously decreased with Zusanli stimulation (neural arc, Fig. 3 top left). The peripheral arc does not seem to change by Zusanli stimulation (Fig. 3 top right). These changes resulted in the decreased AP and SNA at the closed-loop operation point (Fig. 3 bottom).

B. Effects on Dynamic Characteristic

Fig. 4 exemplifies the time series of data obtained before and during pseudorandom changes in CSP. We imposed changes in CSP of ±20 mmHg around the respective closed-loop operating point.

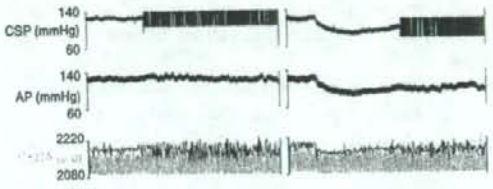

Fig. 4. An example of time series before and during changes in carotid sinus pressure according to pseudorandom binary sequence, with (right) and without (left) electrical acupuncture. CSP, carotid sinus pressure; AP, arterial blood pressure; CSNA, cardiac sympathetic nerve activity

Changes in dynamic characteristics of neural arc, peripheral arc, and total loop by electrical acupuncture are shown in Fig. 5. As shown in the figure, transfer functions (dynamic characteristics) of neural arc, peripheral arc, and total loop were superimposable.

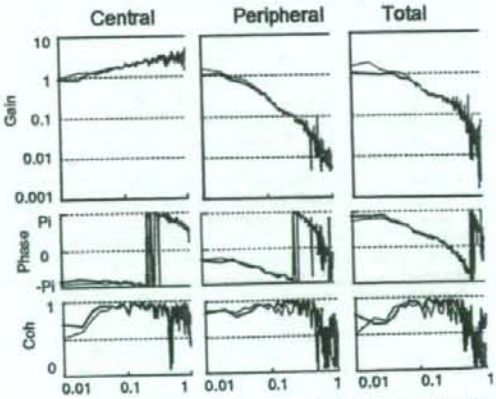

Fig. 5. Transfer functions (dynamic characteristics) of neural arc (left), peripheral arc (middle), and total loop (right) of baroreflex, with (gray) and without (black) electrical acupuncture. From top to bottom, gain, phase, and squared magnitude of coherence are shown.

IV. Discussion

We have repeatedly demonstrated that electrical vagal stimulation was successful in retarding further deterioration of cardiac function and progression of cardiac remodeling in rats with severe heart failure. This therapeutic method is also capable of prolonging survival in heart failure rats. These effects were believed to be mediated by the modification of autonomic balance.

Based on these results, several groups of investigators are developing an implantable vagal neurostimulators to apply this method for the human use; the invasive nature of the implantable device is likely to limit its widespread use, especially in relatively mild cases of heart failure.

A less invasive measure is definitely needed. To develop a less invasive method for modifying autonomic balance, we have examined the effect of Zusanli electrical stimulation. This method has been used to treat various diseases in oriental medicine.

To ensure these effects of traditional medicine, we have conducted animal experiments. The results have shown depressor and sympathetic neuroinhibitory (static) effect during Zusanli electrical stimulation. These effects are mediated by the changes in neural arc. We have also demonstrated that dynamic characteristics of baroreflex neural and peripheral arcs did not change by Zusanli electrical stimulation. We conclude that application of electrical acupuncture can suppress sympathetic nerve activity but does not affect the dynamic characteristics of the arterial baroreflex system, indicating no deleterious effect on orthostatic tolerance.

References

[1] M. Li, C. Zheng, T. Sato, T. Kawada, M. Sugimachi, K. Sunagawa. "Vagal nerve stimulation markedly improves long-term survival after chronic heart failure in rats." *Circulation.* Vol. 109, pp. 120-124, Jan. 2004.

[2] T. Sato, T. Kawada, M. Inagaki, T. Shishido, H. Takaki, M. Sugimachi, K. Sunagawa, "New analytic framework for understanding sympathetic baroreflex control of arterial pressure." *Am. J. Physiol. Heart Circ Physiol.* vol. 276, no. 6, pp. H2251-H2261, Jun. 1999.

[3] P. Z. Marmarelis and V. Z. Marmarelis, Analysis of Physiological Systems: The White-Noise Approach, New York, NY: Plenum, 1978.

[4] J. S. Bendat, and A. G. Piersol, Random Data: Analysis & Measurement Procedures, 3rd Ed., New York, NY: Wiley-Interscience, 2000

[5] D. Michikami, A. Kamiya, T. Kawada, M. Inagaki, T. Shishido, K. Yamamoto, H. Ariumi, S. Iwase, J. Sugenoya, K. Sunagawa, M. Sugimachi. "Short-term electroacupuncture at Zusanli resets the arterial baroreflex neural arc toward lower sympathetic nerve activity." *Am J Physiol Heart Circ Physiol.* vol. 291, pp. H318-H326, Jul. 2006.

Am J Physiol Heart Circ Physiol 295: H1081–H1089, 2008.
First published June 27, 2008; doi:10.1152/ajpheart.00023.2008.

Muscle mechanoreflex augments arterial baroreflex-mediated dynamic sympathetic response to carotid sinus pressure

Kenta Yamamoto,[1,2] Toru Kawada,[2] Atsunori Kamiya,[2] Hiroshi Takaki,[2] Toshiaki Shishido,[2] Kenji Sunagawa,[3] and Masaru Sugimachi[2]

[1]*Consolidated Research Institute for Advanced Science and Medical Care, Waseda University, Tokyo;* [2]*Department of Cardiovascular Dynamics, Advanced Medical Engineering Center, National Cardiovascular Center Research Institute, Osaka; and* [3]*Department of Cardiovascular Medicine, Graduate School of Medical Sciences, Kyushu University, Fukuoka, Japan*

Submitted 8 January 2008; accepted in final form 19 June 2008

Yamamoto K, Kawada T, Kamiya A, Takaki H, Shishido T, Sunagawa K, Sugimachi M. Muscle mechanoreflex augments arterial baroreflex-mediated dynamic sympathetic response to carotid sinus pressure. *Am J Physiol Heart Circ Physiol* 295: H1081–H1089, 2008. First published June 27, 2008; doi:10.1152/ajpheart.00023.2008.—Although the muscle mechanoreflex is one of the pressor reflexes during exercise, its interaction with dynamic characteristics of the arterial baroreflex remains to be quantitatively analyzed. In anesthetized, vagotomized, and aortic-denervated rabbits ($n = 7$), we randomly perturbed isolated carotid sinus pressure (CSP) using binary white noise while recording renal sympathetic nerve activity (SNA) and arterial pressure (AP). We estimated the transfer functions of the baroreflex neural arc (CSP to SNA) and peripheral arc (SNA to AP) under conditions of control and muscle stretch of the hindlimb (5 kg of tension). The muscle stretch increased the dynamic gain of the neural arc while maintaining the derivative characteristics [gain at 0.01 Hz: 1.0 ± 0.2 vs. 1.4 ± 0.6 arbitrary units (au)/mmHg, gain at 1 Hz: 1.7 ± 0.6 vs. 2.7 ± 1.4 au/mmHg; $P < 0.05$, control vs. stretch]. In contrast, muscle stretch did not affect the peripheral arc. In the time domain, muscle stretch augmented the steady-state response at 50 s (−1.1 ± 0.3 vs. −1.7 ± 0.7 au; $P < 0.05$, control vs. stretch) and negative peak response (−2.1 ± 0.5 vs. −3.1 ± 1.5 au; $P < 0.05$, control vs. stretch) in the SNA step response. A simulation experiment using the results indicated that the muscle mechanoreflex would accelerate the closed-loop AP regulation via the arterial baroreflex.

muscle stretch; transfer function; exercise pressor reflex; exercise; arterial pressure

THE ARTERIAL BAROREFLEX SYSTEM plays an important role in stabilizing arterial pressure (AP) during daily activity. Knowledge of the open-loop static and dynamic characteristics of the arterial baroreflex is essential for a systematic understanding of how the baroreflex system regulates AP. The static characteristics provide information on the operating point of the baroreflex system (19, 34, 48), whereas the dynamic characteristics determine the stability and quickness of the baroreflex system (14, 22, 23). Importantly, many previous studies showed that exercise resets the baroreflex function (3, 5, 6, 29, 30, 32, 35, 36, 40, 45, 47). However, only a few investigations focused on the dynamic characteristics of the arterial baroreflex during exercise (10, 36, 38, 57). The dynamic characteristics of the arterial baroreflex determine how quickly or slowly the system would response to baroreceptor pressure perturbations. Such information cannot be obtained from the static characteristics alone.

The neural mechanisms responsible for changes in the baroreflex function during exercise are considered to be mediated by central command (6, 13, 29, 39, 46) and by afferent inputs from metabolic and mechanical-sensitive skeletal muscle receptors (11, 12, 17, 41, 43, 44, 49). Regarding the static interaction between the muscle mechanoreflex and arterial baroreflex, we performed a baroreflex open-loop study and reported that muscle stretch extended the response range of sympathetic nerve activity (SNA) to baroreceptor pressure input (58, 59). Based on the results, we hypothesized that the activation of the muscle mechanoreflex would augment the dynamic SNA response to baroreceptor pressure input under open-loop conditions. To the best of our knowledge, however, the effects of the muscle mechanoreflex on the dynamic characteristics of the arterial baroreflex have never been reported.

To test the above hypothesis, we identified the dynamic characteristics of the baroreflex during muscle stretch in anesthetized rabbits under baroreflex open-loop conditions (14, 22, 23). The transfer functions from baroreceptor pressure input to SNA (the baroreflex neural arc) and from SNA to AP (the baroreflex peripheral arc) were estimated by a white noise approach (51). The "whiteness" is essential for the system identification of the arterial baroreflex because it is equivalent mathematically to test the system with all possible pressure changes within the frequency range of interest.

METHODS

Surgical preparations. Animals were cared for in strict accordance with the Guiding Principles for the Care and Use of Animals in the Field of Physiological Sciences approved by the Physiological Society of Japan. All protocols were approved by the Animal Subjects Committee of the National Cardiovascular Center. Seven Japanese White rabbits weighing 2.6–3.0 kg were anesthetized via an intravenous injection (2 ml/kg) of a mixture of urethane (250 mg/ml) and α-chloralose (40 mg/ml) and were mechanically ventilated with oxygen-enriched room air. Supplemental anesthetics (0.2–0.3 $ml \cdot kg^{-1} \cdot h^{-1}$) were administered continuously to maintain stable AP and heart rate levels during intervals of experimental protocols, which were indicative of an appropriate level of anesthesia. Arterial blood was sampled from the left common carotid artery. Rabbits were slightly hyperventilated to suppress chemoreflexes (arterial P_{CO_2} ranged from 30 to 35 mmHg, arterial $P_{O_2} > 300$ mmHg). Arterial blood pH was within the

Address for reprint requests and other correspondence: K. Yamamoto, Consolidated Research Institute for Advanced Science and Medical Care, Waseda Univ., 513 Wasedatsurumakicho, Shinjuku, Tokyo 162-0041, Japan (e-mail: kenta@aoni.waseda.jp).

The costs of publication of this article were defrayed in part by the payment of page charges. The article must therefore be hereby marked "*advertisement*" in accordance with 18 U.S.C. Section 1734 solely to indicate this fact.

physiological range when examined at the end of the surgical preparation as well as at the end of the experiment. The body temperature of each animal was maintained at ~38°C with a heating pad. AP was measured using a high-fidelity pressure transducer (Millar Instruments, Houston, TX) inserted from the right femoral artery to the aortic arch.

We isolated bilateral carotid sinuses from the systemic circulation by ligating the internal and external carotid arteries and other small branches originating from the carotid sinus region. Isolated carotid sinuses were filled with warmed physiological saline via catheters inserted through the common carotid arteries. Intra-CSP was controlled by a servo-controlled piston pump (model ET-126A, Labworks, Costa Mesa, CA). Bilateral vagal and aortic depressor nerves were sectioned at the neck to minimize reflexes from the cardiopulmonary region and from the aortic arch.

We exposed the left renal sympathetic nerve retroperitoneally and attached a pair of stainless steel wire electrodes (Bioflex wire AS633, Cooner Wire, Chatsworth, CA) to record SNA. The nerve bundle peripheral to the electrodes was tightly ligated and crushed to eliminate afferent signals from the kidney. The nerve and electrodes were secured with silicone glue (Kwik-Sil, World Precision Instruments, Sarasota, FL). The preamplified nerve signal was band-pass filtered at 150–1,000 Hz, full-wave rectified, and low-pass filtered with a cutoff frequency of 30 Hz to quantify the nerve activity.

With the rabbit in the prone position, the sacrum, left ankle, and knee were clamped with a custom-made apparatus to prevent body trunk and hindlimb movement during muscle stretch. The left triceps surae muscle, Achilles tendon, and calcaneus bone were exposed. The left triceps surae muscle was isolated from the surrounding tissue. The Achilles tendon was severed from the calcaneus bone and attached to a force transducer (Load Cell LUR-A-SA1, Kyowa Electronic Instruments, Tokyo, Japan). During muscle stretch, the other side of the force transducer was connected to a 5-kg weight via a pulley.

Protocols. To obtain operating pressure values, the carotid sinus baroreflex negative feedback loop was effectively closed by adjusting CSP to AP. Mean AP (and thus mean CSP) at steady state was treated as the operating pressure under control conditions. We then performed muscle stretch for 1 min while the carotid sinus baroreflex was effectively closed. Mean AP during the last 10 s of muscle stretch was treated as the operating pressure under muscle stretch conditions.

To estimate the baroreflex dynamic characteristics, CSP was assigned either high (+20 mmHg) or low (−20 mmHg) pressure values around the operating pressure according to a binary white noise sequence. The switching interval of the binary white noise signal was set at 500 ms so that the CSP power spectrum was fairly flat up to 1 Hz. We confirmed that the muscle stretch produced a sustained SNA increase for at least 7 min (58). To limit the maximum duration of muscle stretch within this time period, a 6-min CSP perturbation was performed twice using different binary sequences, and the two sets of data were pooled for analyses under both control and muscle stretch conditions. The order of control and muscle stretch conditions was randomized across the animals.

Data analysis. We recorded CSP, muscle tension, SNA, and AP at a sampling rate of 200 Hz using a 12-bit analog-to-digital converter. Data were stored on a dedicated laboratory computer system.

To estimate the neural arc transfer function of the carotid sinus baroreflex, we treated CSP as the input and SNA as the output of the system. In the peripheral arc transfer function, we treated SNA as the input and AP as the output of the system. In the total loop transfer function, we treated CSP as the input and AP as the output of the system. Data analysis was started from 90 s after the initiation of each trial to process the stationary portion of data without the effects of transition from closed-loop CSP waveform to open-loop binary white noise CSP input and the transition from nonstretch to stretch of muscle mechanoreceptors. The input-output data pairs were resampled at 10 Hz and segmented into 50%-overlapping bins of 1,024 points each. For each segment, a linear trend was subtracted, and a Hanning window was applied. A fast Fourier transform was performed to obtain the frequency spectra of the input and output signals. The ensemble averages of input power spectral density [$S_{XX}(f)$], output power spectral density [$S_{YY}(f)$], and cross-spectral density between the input and output [$S_{YX}(f)$] were obtained over eight segments derived from two sets of data, where f represents frequency. Finally, we calculated the transfer function from input to output [$H(f)$] using the following equation (27):

$$H(f) = \frac{S_{YX}(f)}{S_{XX}(f)} \quad (1)$$

Hereinafter, we denote the modulus as the dynamic gain of the transfer function. To quantify the linear dependence between input and output signals in the frequency domain, we calculated a magnitude-squared coherence function [Coh(f)] using the following equation (27):

$$\mathrm{Coh}(f) = \frac{|S_{YX}(f)|^2}{S_{XX}(f)S_{YY}(f)} \quad (2)$$

The coherence value ranges from zero to unity. Unity coherence indicates perfect linear dependence between input and output signals, whereas zero coherence indicates total independence between the two signals.

To facilitate an intuitive understanding of the transfer function, the step response corresponding to the transfer function was also calculated as follows. The system impulse response was derived from the inverse Fourier transform of $H(f)$. The step response was obtained from the time integral of the impulse response.

Statistical analysis. All data are presented as means ± SD. Because the amplitude of SNA varied depending on recording conditions, such as the physical contact between the nerve and electrodes, SNA was presented in arbitrary units (au). Neural and peripheral arc transfer functions were normalized in each animal so that the average gain values below 0.03 Hz in the control trial became unity. To compare the transfer functions between two conditions, a transfer gain value at 0.01 Hz ($G_{0.01}$), 0.1 Hz ($G_{0.1}$), 0.5 Hz ($G_{0.5}$), and 1 Hz (G_1) were calculated. In the step response of the neural arc, the steady-state step response at 50 s (S_{50}), the negative peak value (S_{peak}), and the time to negative peak (T_{peak}) were calculated. The effects of muscle stretch on these parameters were examined using the paired t-test. Differences were considered significant when $P < 0.05$.

RESULTS

Figure 1 shows a typical time series of CSP, muscle tension, SNA, and AP under control (*left*) and muscle stretch (*right*) conditions. Although the same binary sequence was applied for two conditions in each animal, different binary sequences were applied for different animals to reduce possible systematic errors in system identification caused by a bias in whiteness specific to a selected binary sequence. The mean CSP during muscle stretch conditions (Fig. 1, *right*) was set higher than that during the control conditions (Fig. 1, *left*) to mimic the increase in the operating pressure during muscle stretch under baroreflex closed-loop conditions (i.e., the AP increase by muscle stretch increases the mean input pressure to the baroreceptors). Muscle stretch increased mean levels of SNA and AP compared with control conditions during the experiment (Table 1).

Figure 2 shows the transfer functions of the neural (*left*) and peripheral (*right*) arcs estimated under the control and muscle stretch conditions; gain plots (*top*), phase plots (*middle*), and Coh(f) (*bottom*) are also presented. The thin and thick solid lines in Fig. 2 indicate control and muscle stretch conditions, respectively. In the neural arc, the dynamic gain increased as

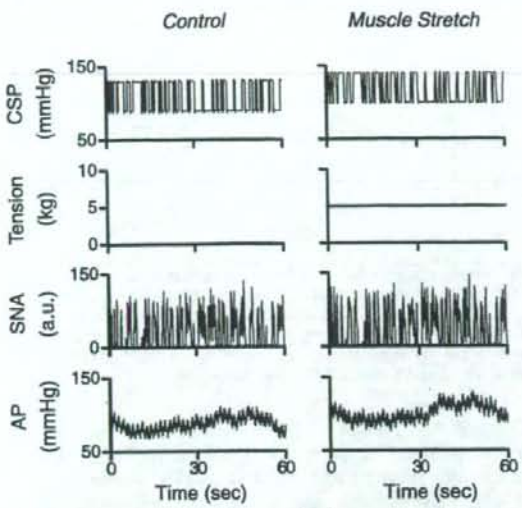

Fig. 1. Typical time series of intracarotid sinus pressure (CSP), muscle tension, sympathetic nerve activity [SNA; in arbitrary units (au)], and arterial pressure (AP) under control (*left*) and muscle stretch (*right*) conditions. CSP was perturbed according to a binary white noise sequence. Muscle stretch increased mean levels of SNA and AP under muscle stretch conditions compared with the control conditions.

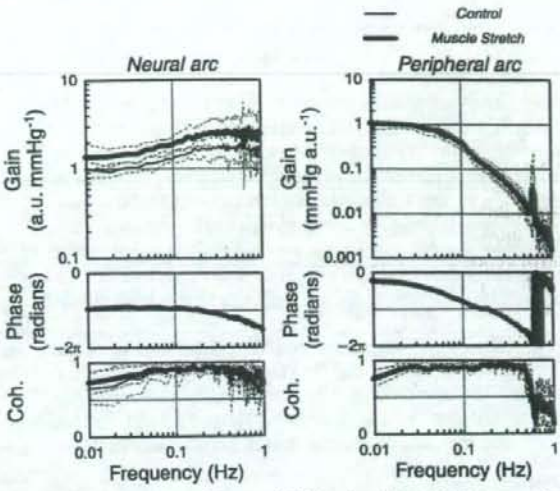

Fig. 2. Transfer functions of the neural (*left*) and peripheral (*right*) arcs under control and muscle stretch conditions. In the neural arc, the input was CSP and the output was SNA. In the peripheral arc, the input was SNA and the output was AP. The mean level of CSP input to the neural arc was set higher under muscle stretch conditions than under control conditions to mimic the physiological condition (i.e., baroreflex closed-loop conditions). Gain plots (*top*), phase plots (*middle*) and coherence (Coh) functions (*bottom*) are shown. Thin and thick solid lines indicate control and muscle stretch conditions, respectively. In the neural arc (*left*), muscle stretch caused an approximately parallel upward shift of the gain plot. Solid and dashed lines represent means and means ± SD values, respectively.

the frequency of input modulation increased under both conditions, indicating derivative characteristics of the neural arc. Muscle stretch caused an approximately parallel upward shift of the gain plot. The phase approached $-\pi$ radians ($-180°$) at the lowest frequency (0.01 Hz) under both conditions, reflecting the negative feedback character of the baroreflex neural arc (i.e., an increase in CSP decreased SNA). Phase plots were nearly superimposed between the two conditions. Coherence values did not differ between both conditions. In the peripheral arc, the dynamic gain decreased in the frequency range from 0.05 to 1 Hz as the frequency of input modulation increased under both conditions, indicating the low-pass characteristics of the peripheral arc. The phase approached 0 radians at the lowest frequency (0.01 Hz) under both conditions, reflecting the fact that an increase in SNA increased AP. The phase lagged with increasing frequency up to 1 Hz. The gain plot, phase plot, and Coh(f) did not differ between both conditions.

Table 1. *Mean levels and CVs of CSP, SNA, and AP at 1, 2, 4, and 6 min under control and muscle stretch conditions*

	Time			
	1 min	2 min	4 min	6 min
		CSP		
Control	95±18	96±18	95±18	96±18
CV	13±2	12±3	11±3	14±2
Muscle stretch	114±15*	115±16*	113±16*	114±15*
CV	11±2	11±1	10±2	12±2
		SNA		
Control	102±4	99±5	100±4	99±4
CV	46±11	45±9	43±9	47±9
Muscle stretch	133±22*	129±21*	127±17*	126±17*
CV	48±11	47±8	44±9	49±10
		AP		
Control	90±21	89±20	88±16	88±18
CV	7±2	6±2	6±2	6±2
Muscle stretch	107±26*	105±22*	104±15*	101±15*
CV	7±3	6±3	6±3	7±2

Values are means ± SD; n = 7. CSP, carotid sinus pressure (in mmHg); SNA, sympathetic nerve activity (in %); AP, arterial pressure (in mmHg); CV, coefficient of variation. Mean and CV values were calculated from 30-s data ending at each time point. *$P < 0.05$ vs. control.

Table 2 summarizes gains of the transfer functions. In the neural arc, $G_{0.01}$, $G_{0.1}$, $G_{0.5}$, and G_1 were higher under muscle

Table 2. *Gains of the transfer functions*

	Control	Muscle Stretch
Neural arc		
$G_{0.01}$, au/mmHg	1.01±0.23	1.44±0.56*
$G_{0.1}$, au/mmHg	1.30±0.11	1.86±0.37*
$G_{0.5}$, au/mmHg	1.77±0.64	2.65±1.08*
G_1, au/mmHg	1.72±0.66	2.72±1.40*
Peripheral arc		
$G_{0.01}$, mmHg/au	1.08±0.06	1.06±0.20
$G_{0.1}$, mmHg/au	0.37±0.09	0.42±0.09
$G_{0.5}$, mmHg/au	0.02±0.01	0.02±0.01
G_1, mmHg/au	0.004±0.001	0.004±0.002
Total loop		
$G_{0.01}$, mmHg/mmHg	1.08±0.18	1.53±0.63*
$G_{0.1}$, mmHg/mmHg	0.48±0.12	0.81±0.31*
$G_{0.5}$, mmHg/mmHg	0.04±0.04	0.06±0.04*
G_1, mmHg/mmHg	0.006±0.003	0.013±0.013

Values are means ± SD; n = 7. $G_{0.01}$, $G_{0.1}$, $G_{0.5}$, and G_1, dynamic gains at 0.01, 0.1, 0.5, and 1 Hz, respectively; au, arbitrary units. *$P < 0.05$ vs. control.

stretch compared with control conditions. In the peripheral arc, $G_{0.01}$, $G_{0.1}$, $G_{0.5}$, and G_1 were unchanged between control and muscle stretch conditions.

Figure 3 shows the total baroreflex loop transfer functions (CSP to AP) under control and muscle stretch conditions. The thin and thick solid lines in Fig. 3 indicate control and muscle stretch conditions, respectively. The dynamic gain decreased as the frequency of input modulation increased under both conditions, indicating low-pass characteristics. The dynamic gain under muscle stretch conditions was higher than that under control conditions in frequency from 0.01 to 0.5 Hz (Table 2). The phase plot and Coh(f) did not differ between both conditions.

Figure 4 shows step responses of SNA corresponding to the transfer functions in the neural arc shown in Fig. 2. The initial drop in the SNA response as well as the steady-state response was augmented during muscle stretch (Table 3). T_{peak} did not differ between control and muscle stretch conditions (Table 3).

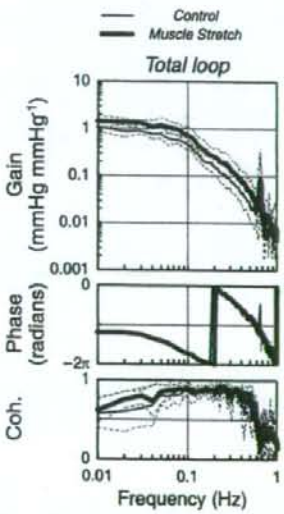

Fig. 3. Total loop transfer functions from CSP to AP under control and muscle stretch conditions. Gain plots (*top*), phase plots (*middle*) and coherence functions (*bottom*) are shown. Thin and thick solid lines indicate control and muscle stretch conditions, respectively. The dynamic gain decreased as the frequency of input modulation increased under both conditions, indicating low-pass characteristics. Muscle stretch caused an approximately parallel upward shift of the gain plot. Solid and dashed lines represent means and means ± SD values, respectively.

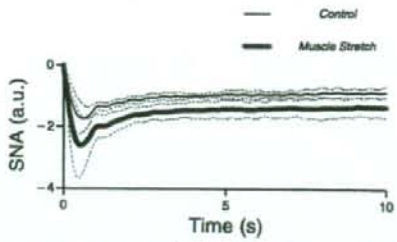

Fig. 4. Step responses corresponding to transfer functions of the neural arc obtained from Fig. 2, showing the SNA response to a 1-mmHg increase in input pressure. Thin and thick solid lines indicate control and muscle stretch conditions, respectively. The initial drop in the SNA response as well as the steady-state response was augmented by the muscle stretch. Solid and dashed lines represent means and means ± SD values, respectively.

DISCUSSION

The key new findings of the present study are as follows. Muscle stretch increased the dynamic gain of the carotid sinus baroreflex neural arc as estimated by binary white noise input (Fig. 2). In contrast, the peripheral arc transfer function remained unchanged irrespective of the muscle stretch (Fig. 2). These results suggest that during muscle mechanoreflex activation, the dynamic SNA response to CSP perturbation is augmented.

System identification by the white noise approach. To identify the dynamic characteristics of arterial baroreflex function quantitatively, we described the carotid sinus baroreflex control of SNA and AP in terms of system identification using the white noise technique. Compared with the traditional approach of testing dynamic properties of the physiological system with step and sine wave stimuli, the white noise approach has definite advantages, as follows (27). First, if a step stimulus is applied, we learn the response of the system to this step and have little notion of the response of the system to any other type of stimulus. If a sinusoidal pulse is applied, then we know the response of the system to such a stimulus and little else. The same applies for any other specific waveform. Theoretically speaking, the system is tested with every possible stimulus in the white noise approach. The white noise stimulus is a very rich stimulus. It should be emphasized that the white noise method is perfectly suited to the analysis of linear systems. As shown in Figs. 2 and 3, high coherence values close to unity indicate the validity of our method for system identification. Second, the identification of the physiological system through the white noise technique is largely unaffected by the types of contaminating noise usually present in such a system. Our study provides the first and quantitative description of the dynamic characteristics of the carotid sinus baroreflex during isolated activation of mechanosensitive afferents from skeletal muscle.

Effects of the muscle mechanoreflex on dynamic characteristics of the carotid sinus baroreflex. The effects of activation of afferents from skeletal muscle, such as those occurring during exercise, on the arterial baroreflex have been extensively studied (5, 13, 29, 42, 43, 49, 58, 59). These studies have demonstrated that the afferent input from muscle resets the baroreflex control of AP, heart rate, and SNA. However, the dynamic characteristics of the arterial baroreflex during isolated activation of muscle mechanosensitive afferents have never been analyzed. In the present study, muscle stretch increased dynamic gain in every frequency (Fig. 2 and Table

Table 3. *Parameters of step responses*

	Control	Muscle Stretch
S_{50}, au	−1.05±0.30	−1.69±0.69*
S_{peak}, au	−2.10±0.50	−3.08±1.45*
T_{peak}, s	0.63±0.21	0.64±0.20

Values are means ± SD; n = 7. A step response is defined as a SNA response to a 1-mmHg change in input pressure. S_{50}, step response at 50 s; S_{peak}, negative peak response; T_{peak}, time to negative peak. *$P < 0.05$ vs. control.

2), whereas it did not affect the peripheral arc. These data are the first to provide quantitative evidence demonstrating that the dynamic SNA response to CSP perturbation is augmented during isolated activation of the muscle mechanoreflex. Although an increase in dynamic gain in the lowest frequency (0.01 Hz) was expected from the results of our previous studies showing an increase in static gain by muscle stretch (58, 59), the information was insufficient to perform a simulation study to examine the effects of muscle stretch on the closed-loop dynamic AP regulation (see *Physiological implications*). The present study extended our previous work by providing additional information on the dynamic interaction over a wide range of frequencies between 0.01 and 1 Hz in the carotid sinus baroreflex.

The static characteristics of the arterial baroreflex determine an operating point of the baroreflex system. Furthermore, the static characteristics described by a modeled sigmoid function provide the parameters of threshold, saturation, and maximal gain at the centering point. However, the static characteristics alone cannot provide the information on the changes over time in the response of the baroreflex system. On the other hand, dynamic analysis techniques such as transfer function analysis estimated by the white noise approach provide information on the stability and quickness of the system response. The dynamic SNA response to baroreceptor pressure input became greater as the frequency of input modulation increased, suggesting derivative characteristics (i.e., high-pass characteristics) of the baroreflex neural arc (Fig. 2, *left*, thin solid line). In contrast, the dynamic AP response to SNA became smaller as the frequency of SNA modulation increased, indicating low-pass characteristics of the baroreflex peripheral arc (Fig. 2, *right*, thin solid line). The total loop transfer function (CSP to AP) is determined by a product of the neural and peripheral arc transfer functions (Fig. 3, thin solid line). Therefore, the decreasing slope of dynamic gain in the total loop transfer function was shallower than that in the corresponding peripheral arc. In other words, the fast neural arc effectively compensates for the slow peripheral arc to accelerate dynamic AP regulation by the baroreflex negative-feedback loop (14). During muscle stretch, the dynamic gain in the neural arc was increased by ~50% in every frequency under study (Fig. 2 and Table 2), indicating that the derivative characteristics of the neural arc were maintained. As a result, the effect of the neural arc compensating for the slow AP response was preserved during the activation of muscle mechanoreflex (Fig. 3 and Table 2). Furthermore, the total loop dynamic gain was augmented during the muscle stretch due to the upward shift of the neural arc transfer function.

Because we used passive muscle stretch as the input for the muscle mechanoreflex, the physiological significance of the present results should be interpreted carefully. Several studies have examined the arterial baroreflex control of SNA during static and dynamic exercise. Static and heavy dynamic exercise resets the baroreflex control of SNA to higher SNA levels with an increase in its sensitivity (9, 11, 17, 32). On the other hand, mild to moderate dynamic exercise resets the baroreflex control of SNA without any change in its sensitivity (3, 24, 38). Because the muscle mechanoreflex is activated during mild to moderate dynamic exercise (4), our results indicate that the muscle mechanoreflex may contribute to increasing the baroreflex gain of SNA during mild to moderate dynamic exercise. In addition to differences in the measured SNA (renal vs. muscle), analytic methods of baroreflex function, modes of mechanoreflex activation, and/or species between the present study and previous studies, the cardiopulmonary baroreflex should be taken into account. Charkoudian et al. (1) demonstrated that increasing central venous pressure via head-down tilt or saline infusion attenuated the baroreflex sensitivity in the control of SNA. The activation of cardiopulmonary baroreceptors induced by increasing central venous pressure may influence the arterial baroreflex control during dynamic exercise (37). In the present study, however, the cardiopulmonary baroreflex did not operate due to bilateral vagotomy.

Previous studies (7, 25) have suggested that the muscle mechanoreflex has a dominant role in pressor reflexes during muscle contraction in anesthetized or decerebrate cats. Although we believe that the mechanoreflex is one of the pressor reflexes during exercise, the functional importance of the muscle mechanoreflex in cardiovascular regulation during exercise in conscious conditions is debatable. Matsukawa et al. (28) recently reported that blockade of the muscle mechanoreflex by gadolinium did not alter AP responses to isometric exercise in conscious cats. Moreover, they found that gadolinium significantly diminished the pressor responses to passive muscle stretch in anesthetized cats. These observations suggest that, under the experimental design, the muscle mechanoreflex would not be activated during exercise or, even if it was activated, it has no functional importance in cardiovascular responses to exercise in conscious conditions. One criticism for the study is that there is always a possibility that changes in the central command in conscious conditions had compensated for the lack of muscle mechanoreflex. Further studies are needed to better understand the role of the muscle mechanoreflex on neural cardiovascular responses during exercise.

High-pass characteristics of the baroreflex neural arc. It is likely that the dynamic characteristics of the baroreflex neural arc actually reflect the intrinsic and synaptic properties of central nervous system neurons and neural circuits that transmit baroreceptor input. However, the central baroreceptor synapses are characterized as a low-pass filter (26). The difference between high-pass characteristics of the neural arc transfer gain and low-pass characteristics of the central baroreceptor synaptic transmission could be attributable to the difference of estimated frequency ranges. Frequency-dependent depression (FFD) of synaptic transmission in the baroreflex central pathways is the phenomenon that the probability of excitatory postsynaptic potentials progressively reduces as the frequency of afferent input increases beyond 1 Hz (2, 33). Although FDD and transfer gain should be discriminated in theory, interactions between FDD and transfer gain may occur when the modulation frequency of afferent fiber stimulation approached the frequency range of FDD. Indeed, Kawada et al. (23) found high-cut characteristics of the baroreflex neural arc in the frequency range above ~1 Hz. In the present study, the transfer gain was derived from 0.01 to 1 Hz. Whether the dynamic interaction between carotid sinus baroreflex and muscle mechanoreflex exists in the frequency range beyond 1 Hz awaits further studies.

Part of the high-pass characteristics in the baroreflex neural arc is attributable to the derivative nature observed in the baroreceptor transduction from CSP input to baroreceptor afferent nerve activity (i.e., mechanoneural transduction) (21).

However, we think there exists high-pass characteristics in the transduction from baroreceptor afferent input to efferent SNA, because the magnitude of high-pass characteristics slightly differs between cardiac and renal SNAs in response to the same baroreceptor pressure perturbation (18).

In an electrical circuit, we can design a high-pass filter only from low-pass filter elements using a feedback loop (Fig. 5). Although the main forward path of the baroreflex neural arc from afferent nerve activity to efferent SNA is considered to be the nucleus tractus solitarius, caudal ventrolateral medulla, and rostral ventrolateral medulla (53), there could be feedback connections between these areas. Therefore, it is possible that synaptic connection has basically low-pass characteristics, whereas the baroreflex neural arc reveals high-pass characteristics as a neural circuit. The speculation also needs to be verified experimentally in the future.

Physiological implications. Under physiological conditions, the baroreflex is closed as a negative feedback system. In the following discussion, we will focus on the effect of the augmentation of dynamic SNA modulation in the neural arc on the closed-loop dynamic AP regulation. Figure 6*A* illustrates a simulator consisting of the linear neural arc transfer function (H_N) and linear peripheral arc transfer function (H_P) followed by the nonlinear sigmoidal components (see the APPENDIX for details). A closed-loop AP response to a stepwise pressure perturbation (−40 mmHg) with pulsatile pressure was simulated, and the result is shown in Fig. 6*B*. Muscle stretch shortened the time to 95% of steady state by ~33% from 7.2 to 4.8 s (shaded and solid arrows in Fig. 6*B*). This result suggests that, under baroreflex closed-loop conditions, the rate of recovery in AP following a pressure perturbation occurs sooner when accompanied by the muscle mechanoreflex. Increasing the quickness of the negative-feedback system can be caused by augmentation and/or acceleration of the open-loop transfer function of the system. In our baroreflex open-loop experiment, S_{50} and S_{peak} in the step responses of SNA were augmented by the muscle stretch (Fig. 4 and Table 3). On the other hand, T_{peak} did not differ between control and muscle stretch conditions (Fig. 4 and Table 3). These results suggest that the improvement in the quickness of the AP restoration via the baroreflex observed in the closed-loop simulation was induced by augmentation, rather than acceleration, of the dynamic SNA response in the neural arc. However, further experimental studies are needed to verify the simulation model.

Limitations. The present study has several limitations. First, we performed the experiment in anesthetized animals. Previous studies have suggested that any anesthetic could alter the baroreflex regulation in AP (54–56). The gain of the baroreflex is reported in the conscious state to be higher (~2-fold) than in the anesthetized state. A previous study (52) suggested that α-chloralose anesthesia could alter the dynamic characteristics of the baroreflex regulation around the frequency of 5 Hz. However, the anesthesia was convenient for the elimination of the central command. Furthermore, we compared the baroreflex gain between muscle stretch and nonstretch conditions both under anesthesia. Therefore, a reasonable interpretation would be that the increased baroreflex gain is attributable to muscle stretch in this experiment.

Second, stretching of skeletal muscle provides a stimulus for the activation of mechanoreceptors that is different from that which occurs during muscle contraction. During contraction, mechanoreceptors are activated by a shortening of skeletal muscle and by compression of the receptors. Thus, mechanoreceptors may be stimulated in a very different manner during stretch, which would likely affect the magnitude of the corresponding reflex response. In addition, the level of muscle stretch used in our experiment was relatively high (50). The stretch may activate different afferents than contraction (8). Furthermore, the discharge profile of mechanosensitive afferents adapt during static muscle stretch (31). Accordingly, during the muscle stretch for 6 min in the present study, the firing level from the mechanoreceptors might have been

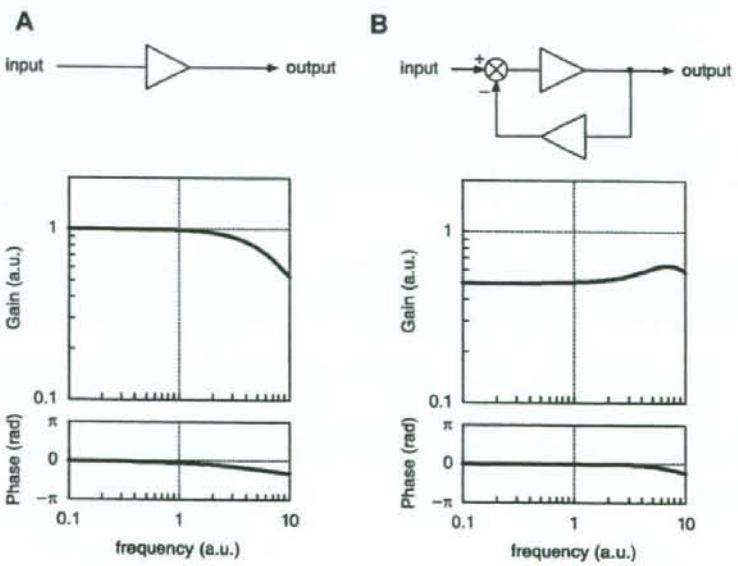

Fig. 5. An example that a circuit consisting of only low-pass elements yields high-pass characteristics as a circuit. *A*: block diagram of a single low-pass element (triangle) and its transfer function. Units for gain and frequency are arbitrary. *B*: block diagram of a circuit with a negative feedback loop with the same low-pass element (triangles). Because gain in the lower frequency range is attenuated more by the low-pass characteristics of the feedback path, the transfer function from input to output reveals high-pass characteristics.

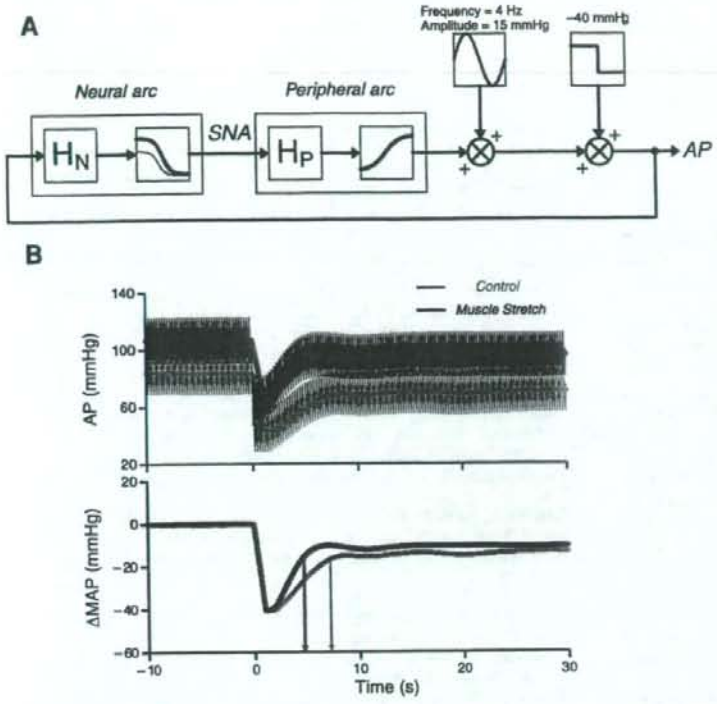

Fig. 6. *A*: simulator of the baroreflex system during activation of the muscle mechanoreflex. A stepwise perturbation with pulsatile pressure was applied to the baroreflex negative feedback system (see the APPENDIX for details). H_N, neural arc transfer function; H_P, peripheral arc transfer function. *B*: simulation results of the closed-loop AP response to the stepwise pressure perturbation (−40 mmHg). Muscle stretch shortened the time to 95% of steady state by ~33% (shaded and solid arrows). Shaded and solid thick lines indicate mean AP (MAP) resampled at 1 Hz. ΔMAP, change in MAP from baseline.

steadily diminishing. In fact, the increase in SNA and AP induced by muscle stretch gradually decreased from 90 s to 6 min after the initiation of the muscle stretch, which was used for data analysis (Table 1). However, SNA and AP remained significantly higher under muscle stretch conditions than control conditions over the protocol for 6 min. Thus, we believe that the mechanoreflex remained activated in this protocol. Further studies are required to elucidate the dynamic interactions between baroreflex and mechanoreflex induced by different modes of activation, such as cyclic activation of the mechanoreflex.

Third, the transfer function analysis is useful in identifying the linear input-output relationship of the baroreflex at a given operating point. However, the transfer function cannot characterize the nonlinear input-output relationship of the system. In the presence of nonlinear system behavior such as the baroreflex system, the transfer function analysis is partly compromised, indicating that the absolute output values of the nonlinear system to given input signals cannot be predicted accurately by the transfer function alone. Combining a linear transfer function with a nonlinear sigmoidal element would increase the accuracy to reproduce dynamic characteristics observed in the baroreflex neural arc (20, 22).

Finally, we measured renal SNA as a proxy of systemic sympathetic activity. SNAs to different organs may vary a lot. Although static and dynamic regulations of the baroreflex neural arc are similar among renal, cardiac, and muscle SNAs (15, 16, 18), whether this holds true during muscle stretch remains to be verified. Also, subsystems of the peripheral arc transfer function such as those relating cardiac output and peripheral vascular resistance remain to be identified.

Conclusions. In conclusion, baroreflex open-loop transfer function analysis demonstrated that the activation of mechanosensitive afferents from skeletal muscles augmented the dynamic SNA response in the neural arc. This augmentation of the dynamic SNA response with maintained derivative characteristics of the neural arc may accelerate closed-loop AP regulation via the baroreflex.

APPENDIX

To simulate the closed-loop AP response to stepwise pressure perturbation (Fig. 6), we used the derivative-sigmoidal cascade model. The cascade model consists of a linear derivative filter followed by a nonlinear sigmoidal component (20, 22).

We modeled the sigmoidal nonlinearity in the baroreflex neural arc interacting with the muscle mechanoreflex by the following four-parameter logistic function with threshold according to a previous study (59):

$$y = \max\left\{\frac{P_1}{1+\exp[P_2(x-P_3)]} + P_4,\ \mathrm{Th}\right\} \qquad (A1)$$

where x and y are input (in mmHg) and output (in au) values. P_1 denotes the response range (in au), P_2 is the coefficient of gain, P_3 is the midpoint of the input range (in mmHg), P_4 is the minimum output value of the symmetric sigmoid curve (in au), and Th is a threshold value for the output (in au). The function $\max\{a,b\}$ gives the greater or equal value between a and b. We set P_1 = 135 au, P_2 = 0.13, P_3 = 110 mmHg, P_4 = −40 au, and Th = 0 au. Under muscle stretch conditions, the value of P_4 was changed to 5 au. These settings were determined based on the static interaction

between the baroreflex and muscle mechanoreflex obtained from previous studies (58, 59).

The sigmoidal nonlinearity in the peripheral arc was modelled by a four-parameter logistic function as follows:

$$z = \frac{Q_1}{1 + \exp[Q_2(y - Q_3)]} + Q_4 \qquad (A2)$$

where y and z are input (in au) and output (in mmHg) values. Q_1 denotes the response range (in mmHg), Q_2 is the coefficient of gain, Q_3 is the midpoint of the input range (in au), and Q_4 is the minimum output value (in mmHg). We set $Q_1 = 120$ mmHg, $Q_2 = -0.05$, $Q_3 = 70$ au, and $Q_4 = 30$ mmHg under both conditions, according to a previous study (58).

The neural arc (H_N) and peripheral arc (H_P) linear transfer functions under control and muscle stretch conditions were obtained from Fig. 2. Because absolute values of the steady-state gains in the neural and peripheral arcs were determined by a sigmoid curve (*Eqs. A1* and *A2*), the steady-state gains of H_N and H_P under both conditions were normalized to unity.

The input amplitude of the stepwise pressure perturbation was −40 mmHg. To mimic pulsatile pressure, we imposed a sinusoidal input on the output from the peripheral arc. The frequency and zero to peak amplitude of the sinusoidal input were 4 Hz and 15 mmHg, respectively (Fig. 6*A*). The closed-loop AP response was simulated up to 30 s (Fig. 6*B*).

GRANTS

This work was supported by Ministry of Health, Labour and Welfare of Japan Health and Labour Sciences Research Grant for Research on Advanced Medical Technology, Health and Labour Sciences Research Grant for Research on Medical Devices for Analyzing, Supporting and Substituting the Function of Human Body, and Health and Labour Sciences Research Grants H18-Iryo-Ippan-023 and H18-Nano-Ippan-003; the Industrial Technology Research Grant Program of the New Energy and Industrial Technology Development Organization of Japan; and Ministry of Education, Culture, Sports, Science and Technology Grant-In-Aid for Scientific Research 18591992.

REFERENCES

1. **Charkoudian N, Martin EA, Dinenno FA, Eisenach JH, Dietz NM, Joyner MJ.** Influence of increased central venous pressure on baroreflex control of sympathetic activity in humans. *Am J Physiol Heart Circ Physiol* 287: H1658–H1662, 2004.
2. **Chen CY, Horowitz JM, Bonham AC.** A presynaptic mechanism contributes to depression of autonomic signal transmission in NTS. *Am J Physiol Heart Circ Physiol* 277: H1350–H1360, 1999.
3. **Fadel PJ, Ogoh S, Watenpaugh DE, Wasmund W, Olivencia-Yurvati A, Smith ML, Raven PB.** Carotid baroreflex regulation of sympathetic nerve activity during dynamic exercise in humans. *Am J Physiol Heart Circ Physiol* 280: H1383–H1390, 2001.
4. **Gallagher KM, Fadel PJ, Smith SA, Norton KH, Querry RG, Olivencia-Yurvati A, Raven PB.** Increases in intramuscular pressure raise arterial blood pressure during dynamic exercise. *J Appl Physiol* 91: 2351–2358, 2001.
5. **Gallagher KM, Fadel PJ, Stromstad M, Ide K, Smith SA, Querry RG, Raven PB, Secher NH.** Effects of exercise pressor reflex activation on carotid baroreflex function during exercise in humans. *J Physiol* 533: 871–880, 2001.
6. **Gallagher KM, Fadel PJ, Stromstad M, Ide K, Smith SA, Querry RG, Raven PB, Secher NH.** Effects of partial neuromuscular blockade on carotid baroreflex function during exercise in humans. *J Physiol* 533: 861–870, 2001.
7. **Hayes SG, Kaufman MP.** Gadolinium attenuates exercise pressor reflex in cats. *Am J Physiol Heart Circ Physiol* 280: H2153–H2161, 2001.
8. **Hayes SG, Kindig AE, Kaufman MP.** Comparison between the effect of static contraction and tendon stretch on the discharge of group III and IV muscle afferents. *J Appl Physiol* 99: 1891–1896, 2005.
9. **Ichinose M, Saito M, Fujii N, Ogawa T, Hayashi K, Kondo N, Nishiyasu T.** Modulation of the control of muscle sympathetic nerve activity during incremental leg cycling. *J Physiol* 586: 2753–2766, 2008.
10. **Ichinose M, Saito M, Kondo N, Nishiyasu T.** Time-dependent modulation of arterial baroreflex control of muscle sympathetic nerve activity during isometric exercise in humans. *Am J Physiol Heart Circ Physiol* 290: H1419–H1426, 2006.
11. **Ichinose M, Saito M, Wada H, Kitano A, Kondo N, Nishiyasu T.** Modulation of arterial baroreflex control of muscle sympathetic nerve activity by muscle metaboreflex in humans. *Am J Physiol Heart Circ Physiol* 286: H701–H707, 2004.
12. **Ichinose M, Saito M, Wada H, Kitano A, Kondo N, Nishiyasu T.** Modulation of arterial baroreflex dynamic response during muscle metaboreflex activation in humans. *J Physiol* 544: 939–948, 2002.
13. **Iellamo F, Legramante JM, Raimondi G, Peruzzi G.** Baroreflex control of sinus node during dynamic exercise in humans: effects of central command and muscle reflexes. *Am J Physiol Heart Circ Physiol* 272: H1157–H1164, 1997.
14. **Ikeda Y, Kawada T, Sugimachi M, Kawaguchi O, Shishido T, Sato T, Miyano H, Matsuura W, Alexander J Jr, Sunagawa K.** Neural arc of baroreflex optimizes dynamic pressure regulation in achieving both stability and quickness. *Am J Physiol Heart Circ Physiol* 271: H882–H890, 1996.
15. **Kamiya A, Kawada T, Yamamoto K, Michikami D, Ariumi H, Miyamoto T, Shimizu S, Uemura K, Aiba T, Sunagawa K, Sugimachi M.** Dynamic and static baroreflex control of muscle sympathetic nerve activity (SNA) parallels that of renal and cardiac SNA during physiological change in pressure. *Am J Physiol Heart Circ Physiol* 289: H2641–H2648, 2005.
16. **Kamiya A, Kawada T, Yamamoto K, Michikami D, Ariumi H, Miyamoto T, Uemura K, Sugimachi M, Sunagawa K.** Muscle sympathetic nerve activity averaged over 1 minute parallels renal and cardiac sympathetic nerve activity in response to a forced baroreceptor pressure change. *Circulation* 112: 384–386, 2005.
17. **Kamiya A, Michikami D, Fu Q, Niimi Y, Iwase S, Mano T, Suzumura A.** Static handgrip exercise modifies arterial baroreflex control of vascular sympathetic outflow in humans. *Am J Physiol Regul Integr Comp Physiol* 281: R1134–R1139, 2001.
18. **Kawada T, Shishido T, Inagaki M, Tatewaki T, Zheng C, Yanagiya Y, Sugimachi M, Sunagawa K.** Differential dynamic baroreflex regulation of cardiac and renal sympathetic nerve activities. *Am J Physiol Heart Circ Physiol* 280: H1581–H1590, 2001.
19. **Kawada T, Shishido T, Inagaki M, Zheng C, Yanagiya Y, Uemura K, Sugimachi M, Sunagawa K.** Estimation of baroreflex gain using a baroreflex equilibrium diagram. *Jpn J Physiol* 52: 21–29, 2002.
20. **Kawada T, Uemura K, Kashihara K, Kamiya A, Sugimachi M, Sunagawa K.** A derivative-sigmoidal model reproduces operating point-dependent baroreflex neural arc transfer characteristics. *Am J Physiol Heart Circ Physiol* 286: H2272–H2279, 2004.
21. **Kawada T, Yamamoto K, Kamiya A, Ariumi H, Michikami D, Shishido T, Sunagawa K, Sugimachi M.** Dynamic characteristics of carotid sinus pressure-nerve activity transduction in rabbits. *Jpn J Physiol* 55: 157–163, 2005.
22. **Kawada T, Yanagiya Y, Uemura K, Miyamoto T, Zheng C, Li M, Sugimachi M, Sunagawa K.** Input-size dependence of the baroreflex neural arc transfer characteristics. *Am J Physiol Heart Circ Physiol* 284: H404–H415, 2003.
23. **Kawada T, Zheng C, Yanagiya Y, Uemura K, Miyamoto T, Inagaki M, Shishido T, Sugimachi M, Sunagawa K.** High-cut characteristics of the baroreflex neural arc preserve baroreflex gain against pulsatile pressure. *Am J Physiol Heart Circ Physiol* 282: H1149–H1156, 2002.
24. **Keller DM, Fadel PJ, Ogoh S, Brothers RM, Hawkins M, Olivencia-Yurvati A, Raven PB.** Carotid baroreflex control of leg vasculature in exercising and non-exercising skeletal muscle in humans. *J Physiol* 561: 283–293, 2004.
25. **Leshnower BG, Potts JT, Garry MG, Mitchell JH.** Reflex cardiovascular responses evoked by selective activation of skeletal muscle ergoreceptors. *J Appl Physiol* 90: 308–316, 2001.
26. **Liu Z, Chen CY, Bonham AC.** Frequency limits on aortic baroreceptor input to nucleus tractus solitarii. *Am J Physiol Heart Circ Physiol* 278: H577–H585, 2000.
27. **Marmarelis PZ, Marmarelis VZ.** The white noise method in system identification. In: *Analysis of Physiological Systems*. New York: Plenum, 1978, p. 131–221.
28. **Matsukawa K, Nakamoto T, Inomoto A.** Gadolinium does not blunt the cardiovascular responses at the onset of voluntary static exercise in cats: a predominant role of central command. *Am J Physiol Heart Circ Physiol* 292: H121–H129, 2007.

29. **McIlveen SA, Hayes SG, Kaufman MP.** Both central command and exercise pressor reflex reset carotid sinus baroreflex. *Am J Physiol Heart Circ Physiol* 280: H1454–H1463, 2001.
30. **Melcher A, Donald DE.** Maintained ability of carotid baroreflex to regulate arterial pressure during exercise. *Am J Physiol Heart Circ Physiol* 241: H838–H849, 1981.
31. **Mense S, Stahnke M.** Responses in muscle afferent fibres of slow conduction velocity to contractions and ischaemia in the cat. *J Physiol* 342: 383–397, 1983.
32. **Miki K, Yoshimoto M, Tanimizu M.** Acute shifts of baroreflex control of renal sympathetic nerve activity induced by treadmill exercise in rats. *J Physiol* 548: 313–322, 2003.
33. **Miles R.** Frequency dependence of synaptic transmission in nucleus of the solitary tract in vitro. *J Neurophysiol* 55: 1076–1090, 1986.
34. **Mohrman DE, Heller LJ.** Regulation of arterial pressure. In: *Cardiovascular Physiology* (4th ed.). New York: McGraw-Hill, 1997, p. 158–230.
35. **Norton KH, Boushel R, Strange S, Saltin B, Raven PB.** Resetting of the carotid arterial baroreflex during dynamic exercise in humans. *J Appl Physiol* 87: 332–338, 1999.
36. **Ogoh S, Fisher JP, Dawson EA, White MJ, Secher NH, Raven PB.** Autonomic nervous system influence on arterial baroreflex control of heart rate during exercise in humans. *J Physiol* 566: 599–611, 2005.
37. **Ogoh S, Fisher JP, Fadel PJ, Raven PB.** Increases in central blood volume modulate carotid baroreflex resetting during dynamic exercise in humans. *J Physiol* 581: 405–418, 2007.
38. **Ogoh S, Fisher JP, Raven PB, Fadel PJ.** Arterial baroreflex control of muscle sympathetic nerve activity in the transition from rest to steady-state dynamic exercise in humans. *Am J Physiol Heart Circ Physiol* 293: H2202–H2209, 2007.
39. **Ogoh S, Wasmund WL, Keller DM, AOY, Gallagher KM, Mitchell JH, Raven PB.** Role of central command in carotid baroreflex resetting in humans during static exercise. *J Physiol* 543: 349–364, 2002.
40. **Papelier Y, Escourrou P, Gauthier JP, Rowell LB.** Carotid baroreflex control of blood pressure and heart rate in men during dynamic exercise. *J Appl Physiol* 77: 502–506, 1994.
41. **Papelier Y, Escourrou P, Helloco F, Rowell LB.** Muscle chemoreflex alters carotid sinus baroreflex response in humans. *J Appl Physiol* 82: 577–583, 1997.
42. **Potts JT, Hand GA, Li J, Mitchell JH.** Central interaction between carotid baroreceptors and skeletal muscle receptors inhibits sympathoexcitation. *J Appl Physiol* 84: 1158–1165, 1998.
43. **Potts JT, Li J.** Interaction between carotid baroreflex and exercise pressor reflex depends on baroreceptor afferent input. *Am J Physiol Heart Circ Physiol* 274: H1841–H1847, 1998.
44. **Potts JT, Mitchell JH.** Rapid resetting of carotid baroreceptor reflex by afferent input from skeletal muscle receptors. *Am J Physiol Heart Circ Physiol* 275: H2000–H2008, 1998.
45. **Potts JT, Shi XR, Raven PB.** Carotid baroreflex responsiveness during dynamic exercise in humans. *Am J Physiol Heart Circ Physiol* 265: H1928–H1938, 1993.
46. **Querry RG, Smith SA, Stromstad M, Ide K, Raven PB, Secher NH.** Neural blockade during exercise augments central command's contribution to carotid baroreflex resetting. *Am J Physiol Heart Circ Physiol* 280: H1635–H1644, 2001.
47. **Rowell LB, O'Leary DS.** Reflex control of the circulation during exercise: chemoreflexes and mechanoreflexes. *J Appl Physiol* 69: 407–418, 1990.
48. **Sato T, Kawada T, Inagaki M, Shishido T, Takaki H, Sugimachi M, Sunagawa K.** New analytic framework for understanding sympathetic baroreflex control of arterial pressure. *Am J Physiol Heart Circ Physiol* 276: H2251–H2261, 1999.
49. **Smith SA, Querry RG, Fadel PJ, Gallagher KM, Stromstad M, Ide K, Raven PB, Secher NH.** Partial blockade of skeletal muscle somatosensory afferents attenuates baroreflex resetting during exercise in humans. *J Physiol* 551: 1013–1021, 2003.
50. **Stebbins CL, Brown B, Levin D, Longhurst JC.** Reflex effect of skeletal muscle mechanoreceptor stimulation on the cardiovascular system. *J Appl Physiol* 65: 1539–1547, 1988.
51. **Sugimachi M, Imaizumi T, Sunagawa K, Hirooka Y, Todaka K, Takeshita A, Nakamura M.** A new method to identify dynamic transduction properties of aortic baroreceptors. *Am J Physiol Heart Circ Physiol* 258: H887–H895, 1990.
52. **Suzuki S, Ando S, Imaizumi T, Takeshita A.** Effects of anesthesia on sympathetic nerve rhythm: power spectral analysis. *J Auton Nerv Syst* 43: 51–58, 1993.
53. **Terui N, Masuda N, Saeki Y, Kumada M.** Activity of barosensitive neurons in the caudal ventrolateral medulla that send axonal projections to the rostral ventrolateral medulla in rabbits. *Neurosci Lett* 118: 211–214, 1990.
54. **Vatner SF, Braunwald E.** Cardiovascular control mechanisms in the conscious state. *N Engl J Med* 293: 970–976, 1975.
55. **Vatner SF, Franklin D, Braunwald E.** Effects of anesthesia and sleep on circulatory response to carotid sinus nerve stimulation. *Am J Physiol* 220: 1249–1255, 1971.
56. **Vatner SF, Franklin D, Van Citters RL, Braunwald E.** Effects of carotid sinus nerve stimulation on blood-flow distribution in conscious dogs at rest and during exercise. *Circ Res* 27: 495–503, 1970.
57. **Wray DW, Fadel PJ, Keller DM, Ogoh S, Sander M, Raven PB, Smith ML.** Dynamic carotid baroreflex control of the peripheral circulation during exercise in humans. *J Physiol* 559: 675–684, 2004.
58. **Yamamoto K, Kawada T, Kamiya A, Takaki H, Miyamoto T, Sugimachi M, Sunagawa K.** Muscle mechanoreflex induces the pressor response by resetting the arterial baroreflex neural arc. *Am J Physiol Heart Circ Physiol* 286: H1382–H1388, 2004.
59. **Yamamoto K, Kawada T, Kamiya A, Takaki H, Sugimachi M, Sunagawa K.** Static interaction between muscle mechanoreflex and arterial baroreflex in determining efferent sympathetic nerve activity. *Am J Physiol Heart Circ Physiol* 289: H1604–H1609, 2005.

Autonomic Neuroscience: Basic and Clinical 144 (2008) 43–49

Contents lists available at ScienceDirect

Autonomic Neuroscience: Basic and Clinical

journal homepage: www.elsevier.com/locate/autneu

Electroacupuncture changes the relationship between cardiac and renal sympathetic nerve activities in anesthetized cats

Hiromi Yamamoto [a,*], Toru Kawada [b], Atsunori Kamiya [b], Toru Kita [a], Masaru Sugimachi [b]

[a] Department of Cardiovascular Medicine, Graduate School of Medicine, Kyoto University, Kyoto 606-8501, Japan
[b] Department of Cardiovascular Dynamics, Advanced Medical Engineering Center, National Cardiovascular Center Research Institute, Osaka 565-8565, Japan

ARTICLE INFO

Article history:
Received 5 June 2008
Received in revised form 13 August 2008
Accepted 12 September 2008

Keywords:
Hind limb stimulation
Baroreflex
Arterial blood pressure
Heart rate

ABSTRACT

Electroacupuncture (EA) is known to affect hemodynamics through modulation of efferent sympathetic nerve activity (SNA), however, possible regional differences in the SNA response to EA remains to be examined. Based on the discordance between arterial blood pressure and heart rate changes during EA, we hypothesized that regional differences would occur among SNAs during EA. To test this hypothesis, we compared changes in cardiac and renal SNAs in response to 1-min EA (10 Hz or 2 Hz) of a hind limb in adult cats anesthetized with pentobarbital sodium. Renal SNA remained decreased for 1 min during EA ($P<0.01$ for both 10 Hz and 2 Hz). In contrast, cardiac SNA tented to decrease only in the beginning of EA. It increased during the end of EA ($P<0.05$ for 2 Hz) and further increased after the end of EA ($P<0.01$ both for 10 Hz and 2 Hz). There was a quasi-linear relationship between renal and cardiac SNAs with a slope of 0.69 (i.e., renal SNA was more suppressed than cardiac SNA) during the last 10 s of EA. The discrepancy between the renal and cardiac SNAs persisted after sinoaortic denervation and vagotomy. In conclusion, EA evokes differential patterns of SNA responses and changes the relationship between cardiac and renal SNAs.

1. Introduction

Electroacupuncture stimulation has been used to modulate autonomic nervous activity and cardiovascular function (Kimura and Sato, 1997; Lin et al., 2001). Several studies have demonstrated that arterial blood pressure (AP) is decreased by acupuncture-like stimulation in anesthetized animals (Kline et al., 1978; Ku and Zou, 1993; Lee and Kim, 1994; Zhou et al., 2005). The cardiovascular responses induced by acupuncture-like stimulation are reflexes mediated via somatic afferent nerves and autonomic efferent nerves (Sato et al., 1994, 2002). Although slow-onset, long-lasting effects may be characteristics of acupuncture, rapid-onset, short-lasting effects are also reported in some experimental conditions. In anesthetized rats, Ohsawa et al. (1995) reported that acupuncture-like stimulation of a hind limb decreased AP in association with a decrease in renal sympathetic nerve activity (RSNA). Uchida et al. (2007) reported that acupuncture-like stimulation of a hind limb induced decreases in cardiac sympathetic nerve activity (CSNA) and heart rate (HR). On the other hand, Kobayashi et al. (1998) reported that acupuncture stimulation produced variable responses including tachycardia, bradycardia, or no responses. We hypothesized that regional differences in sympathetic nerve activities would account for the diverse HR response and more consistent hypotensive response reported during EA. Although Sato et al. (1981) reported that stimulation of group III muscle afferent fibers of a hind limb induces either bradycardic or tachycardic response in anesthetized cats, they did not measure efferent sympathetic nerve activities. To test the hypothesis that EA would evoke regional differences among sympathetic efferent nerve activities, we simultaneously recorded and directly compared CSNA and RSNA during EA in anesthetized cats. The kidneys are important for a long-term AP control via the maintenance of sodium and water balance (DiBona, 2005). At the same time, because the kidneys receive approximately 20% of the cardiac output in resting humans (Rowell, 1974), we thought changes in RSNA could contribute to the acute AP control. We first examined changes in AP, HR, CSNA, and RSNA in response to 10-Hz or 2-Hz EA of a hind limb. We then investigated possible roles of arterial baroreflex and vagal nerve activities in the effects of EA using sinoaortic denervation and vagotomy.

2. Methods

2.1. Surgical preparation

Animal care was provided in strict accordance with the Guiding Principles for the Care and Use of Animals in the Field of Physiological Sciences approved by the Physiological Society of Japan. All protocols were approved by the Animal Subject Committee of National Cardiovascular Center. Adult cats weighing 3.0 to 5.2 kg were anesthetized by an intraperitoneal injection of pentobarbital sodium (30–35 mg/kg) and ventilated mechanically via a tracheal tube with oxygen-supplied room air. The depth of anesthesia was maintained with a continuous intravenous infusion of pentobarbital sodium (1–2 $mg \cdot kg^{-1} \cdot h^{-1}$) through a catheter inserted into the right femoral vein. Vecuronium bromide (0.5–

* Corresponding author. Tel.: +81 75 751 3195; fax: +81 75 751 3203.
E-mail address: hiromi@kuhp.kyoto-u.ac.jp (H. Yamamoto).

1566-0702/$ – see front matter © 2008 Elsevier B.V. All rights reserved.
doi:10.1016/j.autneu.2008.09.002

1.0 mg·kg^{-1}·h^{-1}, i.v.) was given continuously to suppress muscular activity. AP was measured using a catheter-tip manometer inserted from the right femoral artery and advanced into the thoracic aorta. A pair of bipolar stainless steel wire electrodes (AS633, Cooner Wire, Chatsworth, CA) was attached to a branch of the left renal nerve through a flank incision. The nerve fibers peripheral to the electrodes were tightly ligated and crushed to remove afferent signals from the kidney. The nerve fibers and the electrodes were secured with silicone glue (Kwik-Sil, World Precision Instruments, Sarasota, FL). Another pair of bipolar stainless steel wire electrodes was attached to a branch of the left cardiac sympathetic nerve arising from the left stellate ganglion through a resection of the left second rib. The nerve fibers distal to the electrodes were sectioned to eliminate afferent signals from the heart. The nerve fibers and the electrodes were secured with silicone glue. Because the influence of the right cardiac sympathetic nerve on sinus rhythm is greater than that of he left cardiac sympathetic nerve (Yasunaga and Nosaka, 1979), we kept the right cardiac sympathetic nerve intact to preserve the HR response to EA. One rationale for recording left CSNA was that there was no significant laterality in left and right CSNAs during sympathetic perturbation via the arterial baroreflex (Kawada et al., 2003). The preamplified nerve activity signals were band-pass-filtered between 150 and 1000 Hz and then rectified and low-pass-filtered with a cut-off frequency of 30 Hz to quantify CSNA and RSNA. For sinoaortic denervation and vagotomy, we sectioned all nerves surrounding the common carotid arteries at the neck. The carotid sinus nerves were crushed by tight ligatures of 3-0 silk suture around tissues between the internal and external carotid arteries.

2.2. Electroacupuncture

In the supine position, both hind limbs were lifted to obtain a better view of the lateral sides of the lower legs. An EA needle with a diameter of 0.2 mm (CE0123, Seirin-Kasei, Japan) was inserted into a point below the knee joint just lateral to the tibia to the depth of approximately 10 mm. Another EA needle was inserted into the skin behind the ankle as the ground. EA was applied to either the left or right leg using an isolator connected to an electrical stimulator (SEN 7203, Nihon Kohden, Japan). The pulse width was set at 500 μs and the stimulus frequency was set at either 10 or 2 Hz. The stimulus current was set in the range from 2 to 5 mA (2.9±1.1 mA, mean±SD) to produce an AP decrease of more than 5 mmHg at 10-Hz stimulation.

2.3. Protocols

Protocol 1. To examine regional differences in sympathetic nerve activities, we applied 10-Hz or 2-Hz EA for 1 min while measuring AP, HR, CSNA, and RSNA. EA was applied to either the left or right hind limb in random order. An interval of at least 5 min was allowed between the EA trials.

Protocol 2. We applied 10-Hz electrical stimulation to a nonspecific control point in the front of the right thigh to examine whether changes in AP, HR, CSNA, and RSNA observed in Protocol 1 were caused by nonspecific responses to the electrical stimulation.

Protocol 3. To examine possible roles of arterial baroreflex and vagal nerve activities in the effects of EA, we performed sinoaortic denervation and vagotomy. Approximately 20 min after the sinoaortic denervation and vagotomy, changes in AP, HR, CSNA, and RSNA in response to 10-Hz EA were examined.

Protocol 4. To confirm baroreflex-induced changes in sympathetic nerve activity, changes in CSNA and RSNA in response to an intravenous phenylephrine injection (5 μg/kg) were examined before performing sinoaortic denervation and vagotomy. CSNA and

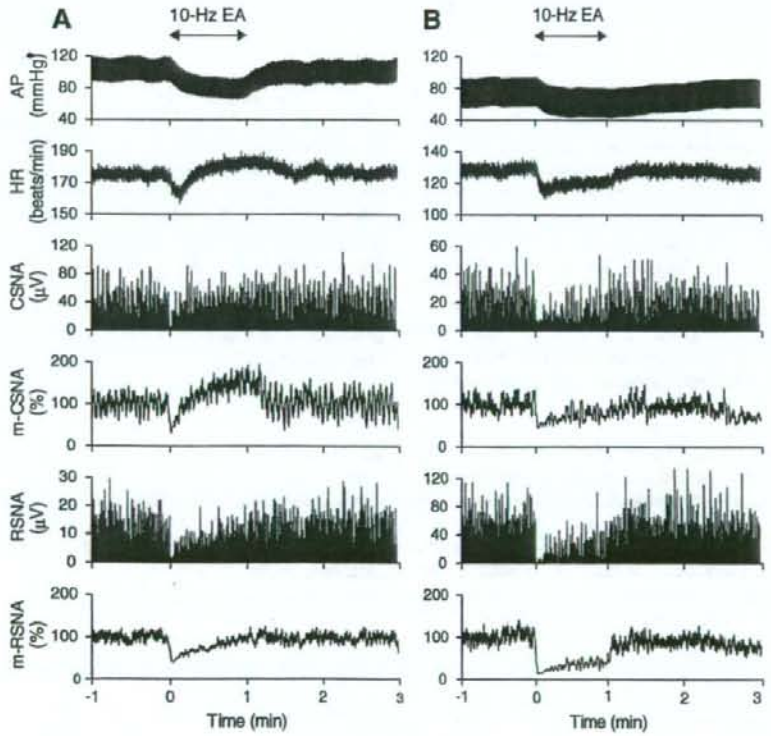

Fig. 1. Time series of arterial pressure (AP), heart rate (HR), cardiac sympathetic nerve activity (CSNA), 2-s moving averaged CSNA (m-CSNA), renal sympathetic nerve activity (RSNA), and 2-s moving averaged RSNA (m-RSNA) during 10-Hz electroacupuncture (EA) obtained from two different animals (see main text for details).